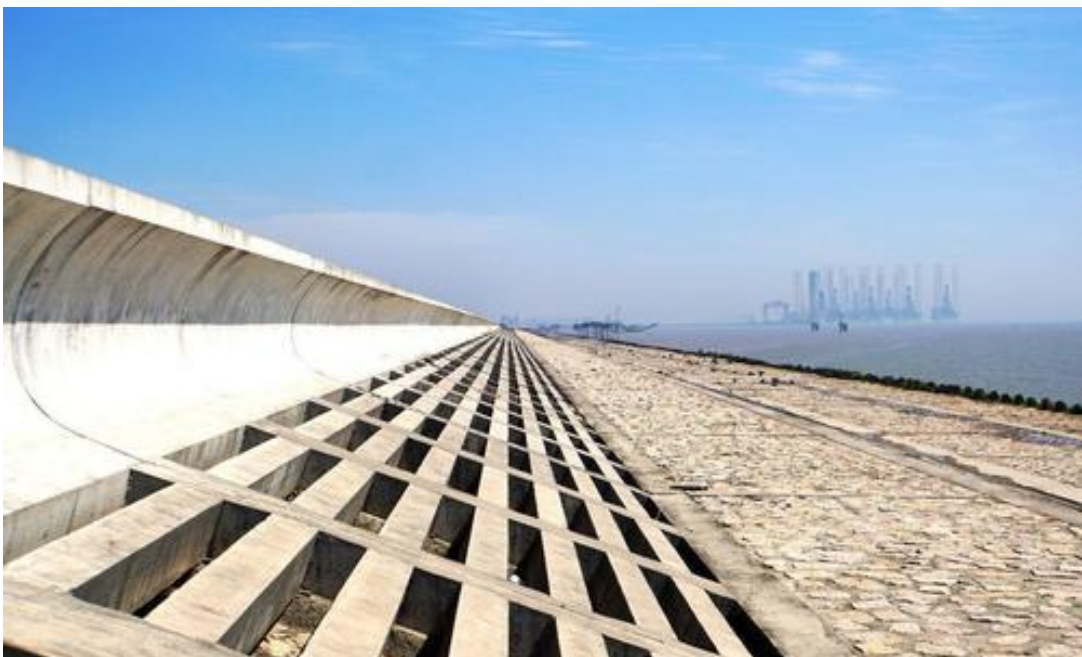


Reliability analysis of sea-dikes in Shanghai city, China



Ruoxi Zhou

October 2020

MSc Thesis

Reliability analysis of sea-dikes

in Shanghai city, China

by

Ruoxi Zhou

Student number: 4824644

Thesis committee: Dr. J. P. Aguilar-López, Delft University of Technology
Dr. R. C. Lanzafame, Delft University of Technology
C. Kuiper, Delft University of Technology
Dr. Q. Ke, Delft University of Technology

Delft University of Technology



Faculty of Civil Engineering and Geosciences (CEG) Hydraulic Engineering
November, 2020

Preface

This work has been carried out to meet the requirements of the Master of Science program in Civil Engineering at Delft University of Technology, the Netherlands.

I would like to give my appreciation to all the members of my graduation committee members. Juan Pablo Aguilar-López, my chairman, encouraged me a lot and gave me a lot of good suggestions on the thesis structure. Robert Lanzafame, my kind and patient daily supervisor, helped me understand how to do academic research, read my reports and helped me with English writing, replied to my email at late nights, always guided me in the right way when I got confused. Coen Kuiper helped me with different kinds of problems I came across during the research, guided me with great patience, gave me valuable advice. Qian Ke gave me a lot information about Shanghai and answered my questions about the data source.

Finally, I sincerely thank all my friends and my parents for giving me love and support.

Ruoxi Zhou November 2020

Summary

Shanghai, one of the busiest and most prosperous metropolises in China, faces big flooding threats due to its unique climatic and geographic characteristics. To protect this city, a system of flood defences were constructed, of which the sea dike system is an important part of the whole flood defence system. Therefore, a reliability analysis of the sea dikes system can give insights into the current safety level by quantifying the probability of sea dike failure, which is the main objective of this study.

The first step was to identify the main failure mechanisms. The overtopping/overflow, revetment instability and macro-instability appeared to be the governing mechanisms. Based on the properties of the three failure mechanisms, the limit state function and corresponding parameters can be derived. Before implementing the calculation of failure probability, the boundary conditions have been analyzed since they are input data for the reliability analysis, which include hydraulic boundary conditions, structural conditions and geotechnical boundary.

Before performing the failure probability calculation, the dike system has been divided into small sections with homogeneous resistance and load parameters to account for the length effect. The failure probability per section per failure mechanism can be derived using the Monte Carlo simulations and they were subsequently combined into the system failure probability ($3.31\text{E-}02$ — $3.64\text{E-}02$). In summary, the overtopping/overflow is the most influential failure mechanism, the failure probability of overtopping/overflow is $3.31\text{E-}02$ (the most vulnerable section: No. 35) for the whole sea dike systems.

To assess the safety level of Shanghai sea dikes, a safety standard needs to be proposed first. However, an optimizing safety level is typically derived from a cost-benefit analysis. This will not be included in this study. The actual safety level of the Shanghai area is less than ($3.31\text{E-}02$ — $3.64\text{E-}02$) per year. Comparison with other low lying densely populated with economical important areas as e.g. The Netherlands where $1/100,000$ per year has been adopted. It is recommended to reconsidered actual safety level and plan dike rehabilitation measures as e.g. strengthening dike inner slope, heightening dike elevation.

Content

PREFACE.....	I
SUMMARY.....	II
CONTENT	III
LIST OF FIGURES.....	VI
LIST OF TABLES	VIII
CHAPTER 1 INTRODUCTION	1
1.1 BACKGROUND	1
1.1.1 Shanghai	1
1.1.2 Floods in Shanghai.....	2
1.1.3 Shanghai Sea Dikes.....	2
1.1.4 Previous research	4
1.2 THESIS OVERVIEW	4
1.2.1 Problem Definition	4
1.2.2 Research Objectives	4
1.2.3 Research Scope.....	5
CHAPTER 2 LITERATURE REVIEW.....	6
2.1 SAFETY ASSESSMENT	6
2.2 PROBABILISTIC ANALYSIS.....	6
2.2.1 Failure Probability.....	6
2.2.2 Reliability Method	7
2.2.3 Fragility Curve	7
2.2.4 Numerical integration	8
2.2.5 Model Uncertainties.....	8
CHAPTER 3 FAILURE MECHANISMS AND DATA ANALYSIS.....	9
3.1 FAILURE MECHANISMS.....	9
3.1.1 Overtopping/overflow	10
3.1.2 Macro-instability	10
3.1.3 Micro-instability.....	11
3.1.4 Piping	11
3.1.5 Revetment failure (erosion of outer slope).....	11
3.1.6 Other Failure Mechanisms	12
3.1.7 Summary	14
3.2 DATA ANALYSIS.....	15
3.2.1 Hydraulic Boundary Conditions	15
3.2.2 Structural Boundary Conditions.....	25
3.2.3 Geotechnical Boundary Conditions	28

CHAPTER 4 CONDITIONAL FAILURE PROBABILITY29

4.1	SECTION DECOMPOSITION	29
4.1.1	Sub-division.....	29
4.1.2	Sub-division decomposition.....	29
4.2	OVERTOPPING/OVERFLOW.....	34
4.2.1	Limit state function	34
4.2.2	Parameters and Distributions.....	37
4.3	INSTABILITY OF AMOUR UNIT	41
4.3.1	Revetment characteristics	42
4.3.2	Limit State Function.....	43
4.3.3	Parameters and Distributions	44
4.4	MACRO INSTABILITY.....	45
4.4.1	Sliding of dike slopes (outer and inner slopes).....	45
4.4.2	Model and software	46
4.4.3	Input data	46
4.4.4	Model set up.....	48
4.5	VARIABLES SUMMARY	48
4.6	CUSTOMIZED MODEL.....	49
4.7	MODEL RESULTS.....	49

CHAPTER 5 SYSTEM RELIABILITY ANALYSIS53

5.1	FAULT TREE.....	53
5.2	CONTRIBUTIONS OF WIND DIRECTION	53
5.2.1	Direction-induced Conditional Failure Probability.....	53
5.2.2	Wind Direction in Shanghai	54
5.2.3	Fragility Curve	58
5.2.4	Failure Probability of the Sub-division	59
5.2.5	Combination of Failure Modes	62
5.3	SENSITIVITY ANALYSIS.....	62
5.4	SAFETY ASSESSMENT.....	63
5.4.1	Safety standard	63
5.4.2	Required level of reliability	68
5.4.3	Risk decrease measures.....	72

CHAPTER 6 CONCLUSIONS AND RECOMMENDATIONS73

6.1	CONCLUSIONS	73
6.1.1	Recognitions about the section decomposition	73
6.1.2	Combination of failure probability	73
6.1.3	Safety assessment.....	74
6.2	RECOMMENDATIONS.....	74
	BIBLIOGRAPHY	76
	APPENDIX A.....	80
	APPENDIX B.....	82
	APPENDIX C	84

List of Figures

Figure 1.1: Shanghai municipality map(Ke, 2014).....	1
Figure 1.2: Districts of the sea dikes in Shanghai	3
Figure 3.1: Schematic overview of the most relevant failure mechanisms of flood defences (S. Jonkman & Schweckendiek, 2015b)	9
Figure 3.2: Example of phreatic line	11
Figure 3.3: Variation of Yangtze River Estuary morphology(J. Zhang et al., 2015)	12
Figure 3.4: Variation of the cross-section in South Channel, Yangtze River Estuary(J. Zhang et al., 2015).....	12
Figure 3.5: Averaged subsidence rate between 2009—2015 (Chen , Yong et al., 2016).....	13
Figure 3.6: Frequency distribution diagram of Shanghai sea dike subsidence rate between 2009—2015 (Chen , Yong et al., 2016)	14
Figure 3.7: Locations of hydrological stations along Shanghai coastline: Wusongkou, Gaoqiao, Sanjiagang, Luchaogang and Jinshanzui. (Shanghai Water Engineering design and Research Institute, 2012)	17
Figure 3.8: Fiting curve of Wusongkou.....	18
Figure 3.9: Locations of meteorological stations.	20
Figure 3.10 :Fitting curves of wind speed (N, Baoshan).....	21
Figure 3.11: Process of wave deformation calculation.	25
Figure 3.12: Crest elevation of Shanghai sea dikes	26
Figure 3.13: Typical cross-section of Shanghai sea dikes	26
Figure 3.14: Orientation of Shanghai sea dikes	27
Figure 4.1: Max. Water level data from 15 August to 21 August in 1997	30
Figure 4.2: Water level variation of three locations (x=0,16,32 km)	31
Figure 4.3: Water level variation of three locations (x=32,38,46)	32
Figure 4.4: Section decomposition.	33
Figure 4.5: Sea embankment with seawall (Ministry of Water Resources, 2014)	35
Figure 4.6: Determination of the average slope (1 st estimate)(Van der Meer et al., 2018).....	39
Figure 4.7: Determination of the average slope (2 nd estimate) (Van der Meer et al., 2018)....	39
Figure 4.8: Configuration of a slope with a storm wall (Van der Meer et al., 2018).....	41
Figure 4.9: Accropode in Shanghai(Yin, 2020a).....	42
Figure 4.10: Fence board in Shanghai(Yin, 2020a).....	43
Figure 4.11: Basic principle of macro-instability (t Hart, De Bruijn, & De Vries, 2016).....	45
Figure 4.12: Assumed circular failure surface in the method of slices(Trompille & Eerninck, 2011)	46
Figure 4.13: Soil layer distribution(Left: Soil layer of Baoshan and Pudong; Right: Soil layer of Nanhui, fengxian and Jinshan)	47
Figure 4.14: Example of phreatic line (Pudong, 10-year return period water level condition).47	
Figure 4.15: Dike geometry of Section 1 as schematized in D-GeoStability	48
Figure 5.1: Fault tree of Shanghai sea dike system.	53
Figure 5.2: Flow chart for the failure of a flood defence system.....	54
Figure 5.3 Location of Section 35.....	55
Figure 5.4 : Example of conditional failure probability (fragility curves) with the respect of water level (Section 77)	58
Figure 5.5 Location of Section 77	59
Figure 5.6: Process of combination(Z. Wang, 2016)	60
Figure 5.7: Risk-based safety standards for flood defences(Slomp et al., 2016)	64
Figure 5.8: Location of Zuid Holland. (Vergouwe, 2016)	64
Figure 5.9: FN curve for flooding of Zuid Holland.(S. N. Jonkman et al., 2008)	66
Figure 5.10: Empirical FN curve (1950-2010) due to historical floods in mainland of China(Ke, 2014)	66
Figure 5.11: From standard to required failure probability per failure mechanism for a representative cross-section(Kok et al., 2017)	68
Figure 5.12: The standard failure probability budget(Kok et al., 2017).....	69

Figure A.1: Schematic illustration of horizontal sliding of the dike body (shearing of the base). The driving force is the horizontal water pressure exerted by the outside water (i.e. river, canal or lake), which may overcome the shear capacity of the dike base(S. Jonkman & Schweckendiek, 2015b).	80
Figure A.2: The overtopping rate of different revetment materials(Fan, 2006).....	82
Figure A.3: Comparison of overtopping numerical results and experiment results.(Yan & Zhang, 2016)	83
Figure B.1: The effect of tidal level change on phreatic line (Left: changing curves of free surface when tide level rises; Right: The changing curves of free surface when tide level drops) (Li, 2015)	84

List of Tables

Table 1.1: Length of sea dikes(Wang , Bo & Xu, 2015).....	3
Table 3.1:Water level for different return periods [WD].	17
Table 3.2: Results of water level frequency analysis.....	19
Table 3.3: Basic information of wind dataset. (<i>Code for Design of Levee Project</i>).	20
Table 3.4: Wind characteristics of Baoshan part (Code for Design of Levee Project).....	20
Table 3.5: Results of statistical performance indicator	22
Table 3.6: Results of probability analysis of wind speed	22
Table 3.7: The fetch and corresponding average water depth(Qiyi & guangwen, 1994)	24
Table 3.8: Cross-section characteristics.....	27
Table 3.9: Orientation division(“orientation” in Table 3.9 stands for the orientation angle of the normal line of the Shanghai sea dikes.)	28
Table 3.10: soil property of South side of the Yangtze River(Cai, 2017).....	28
Table 3.11: soil property of North side of Hangzhou Bay(Cai, 2017)	28
Table 4.1: Summary of water level condition.....	32
Table 4.2: Overview of calculation values for the critical overtopping discharge(en Milieu, 2016b)	36
Table 4.3: Revetment characteristics	43
Table 4.4 : : List of variables	48
Table 4.5: Conditional failure probability of the overtopping under 1000-year water level condition	50
Table 5.1: Summary of the occurrence probability of main wind direction(Shanghai Institute of Building Research Company 2011).....	54
Table 5.2: Conditional failure probability of the sub-division under 1000-year water level condition	56
Table 5.3: Elementary bounds for probability of a series system failure	60
Table 5.4: Elementary bounds of each sub-division of Shanghai sea dikes	60
Table 5.5: Unconditional failure probability of each sub-division.....	62
Table 5.6: Combined failure probability	62
Table 5.7 Sensitivity analysis results.....	63
Table 5.8: Comparison of Shanghai and Zuid Holland.....	67
Table 5.9: The failure probability budget for Shanghai.....	69
Table 5.10: Required failure probability comparison	71
Table 5.11 The comparison of the safety level results of increasing critical discharge or crest elevation	71

Chapter 1 Introduction

This chapter contains an overview of the study, including a short background about Shanghai city and the flood defence system, general information about the reliability analysis, main objectives, and scope of this study.

1.1 Background

1.1.1 Shanghai

Shanghai, one of the metropolises in China, is located at the intersection of China's coastline. Shanghai is a flat and low-lying area which is surrounded by water on four sides, namely the East China Sea (East), the mouth of the Yangtze River (North), the Tai Lake (West) and the Hangzhou Bay (South), as shown in Figure 1.1.

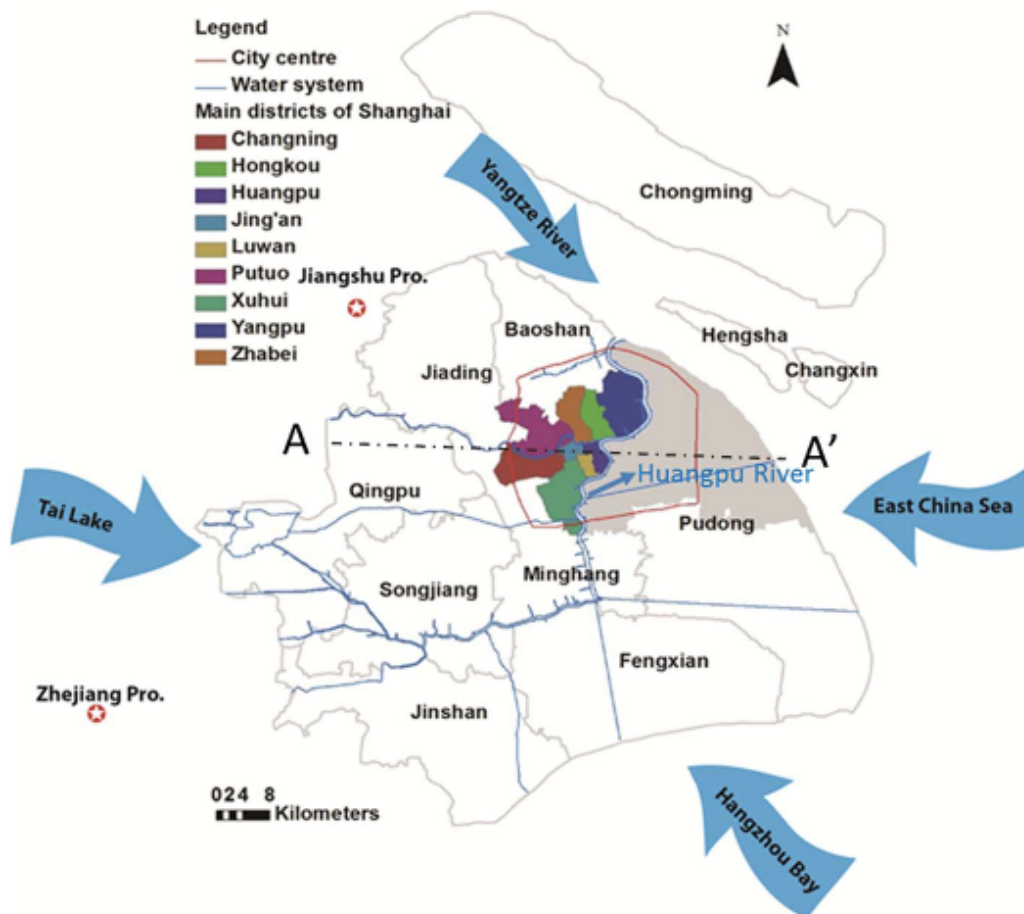


Figure 1.1: Shanghai municipality map(Ke, 2014)

Shanghai has a subtropical monsoon climate, and the average annual rainfall is 1,200 millimeters(Z. Wang, 2016). The annual average temperature of Shanghai is 17.7 °C. The total municipal area of Shanghai is 6341 km², with a resident population of 24.2 million(Statistics, 2018).

1.1.2 Floods in Shanghai

Shanghai experiences great flood risks from sea, river, and lake due to its unique climatic and geographic features. Shanghai is also the most important financial and commercial center in China. Since the economic scale and population density of Shanghai is developing, the flooding will lead to tremendous consequences.

Shanghai experienced many flood disasters for a long time. For example, Typhoon Winnie attacked Shanghai in 1997 and caused significant damage. There was seawater backfilling at Jinshan district since the sea dike of Jinshan part was washed down. 22.6 km long sea dikes were overtopped at Fengxian part(L. Wang, 2019).

In China, floods are usually classified into two different types: overbank flooding and water-logging(S. Du, Gu, Wen, Chen, & Van Rompaey, 2015). The overbank flooding is caused by overflowing of seawaters, rivers, and lakes, while the latter one occurs when the precipitation exceeds evapotranspiration, infiltration and the capacity of the drainage system.

The most conservative identification of the overbank flooding is to identify a flood once water flowing into the backland, while a flood can also be identified by breaching. Breaching can result from many failure modes, like overtopping, overflow, etc. Once the happened breach occurs, water would keep flowing into the land. In this study, coastal flood is mainly considered.

Usually, flooding can be seen as failure of the flood defence line, and this study will focus on the failure of flood defence line due to specific failure mechanisms which cannot withstand the combination of specific hydraulic and geotechnical conditions.

1.1.3 Shanghai Sea Dikes

The Shanghai sea dikes were built from 1949 to 1990s(Chen & Qi, 2010).The total length of sea dikes in Shanghai is 495.8 km which includes the mainland sea dikes(209.9km) and Chongming three island sea dikes(285.9km)(Wang, Bo & Xu, 2015). This research focuses on the mainland part, so only the following districts are involved: Jinshan, Fengxian, Nanhui, Pudong district, Baoshan, shown in Figure 1.2. The length of each district of sea dikes is shown in Table 1.1(Wang, Bo & Xu, 2015). Based on the new Shanghai sea dike plan (2011-2020)(Bureau, 2011), a new standard has been put forward as following: the mainland sea dike has the standard of high water level at the return period of 200 years and 12 level wind.

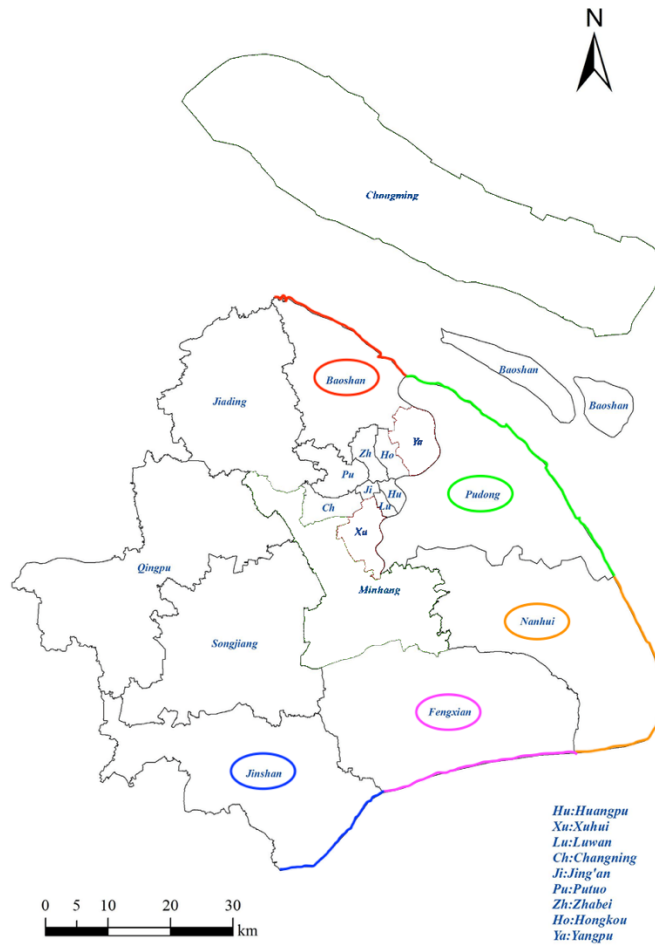


Figure 1.2: Districts of the sea dikes in Shanghai

Table 1.1: Length of sea dikes(Wang , Bo & Xu, 2015)

District	Length [Km]
Baoshan	28.1
Pudong	72.9
Nanhui	43.3
Fengxian	40.8
Jinshan	24.7
Total	209.8

The Shanghai sea defence system consists of sea dikes and sluices. However, the sluices will not be included in this study, so the research object is the dike system. The other detailed data of the sea defence are in Chapter 3.

1.1.4 Previous research

Some researchers did analyses of the reliability of Shanghai sea dikes. Cai analyzed the failure probability of Shanghai sea dikes of three typical cross-sections and his results show that the reliability index β of Shanghai sea dike macro-instability is from 3.21 to 3.91(Cai, 2017). Du calculated the overtopping failure probability of one typical section used the Monte Carlo method and got the result that the failure probability when the overtopping discharge is larger than 50 l/m/s is 8.78×10^{-7} (X. Du, 2013).

1.2 Thesis Overview

1.2.1 Problem Definition

The previous researches of Shanghai sea dikes are mainly only focus on one specific failure mechanism, which cannot give an insight of the real safety level of the Shanghai sea dike system. Therefore, it is required the reliability analysis which takes the local factors of sea dikes into account to calculate the failure probability of the sea-dike system.

So , the main research question is:

How can the reliability of the sea dikes system in Shanghai be quantified?

1.2.2 Research Objectives

The main objective of this study is:

To estimate the failure probability of the system of Shanghai sea dikes by analyzing the individual failure mechanism contributions.

The main objective can be addressed by several sub-questions:

- What failure mechanisms govern the failure probability of Shanghai sea dikes?
- What variables are most influential in the limit state functions?
- What is the current safety level of Shanghai sea dikes system?
- If the failure probability cannot satisfy the requirements, what measures can be taken to improve the reliability of Shanghai sea dikes?

1.2.3 Research Scope

This research focuses on the estimation the failure probability of Shanghai sea-dikes system, taking into account several failure mechanisms. This method follows fully probabilistic approach, in which all relevant parameters for the resistances and the hydraulic loads vary according to specific distributions.

Chapter 2 Literature Review

This Chapter includes the literature review of the safety assessment and methodology that will be used in this study.

2.1 Safety assessment

The Netherlands has always been threatened by floods, so the Dutch government has put a lot of effort on flooding analysis to guarantee the safety of the land. In recent years, the studies called 'the Flood Risk in the Netherlands 2 project' is to estimate the flood risks in the Netherlands, by considering not only the probability of flooding but also its consequences. The risks can be derived by:

$$\text{Risk} = \text{Failure Probability} \cdot \text{Consequence}$$

More and more studies like this led to the new safety standards for flood defences since the beginning of 2017, which are based on flooding probability instead of a design water level which was used in the old safety standard (en Milieu, 2016a).

The failure probability needs to take into account different failure mechanisms and for each failure mechanism a safety assessment method can be used. Similar approaches of calculation of failure probability are used for the Shanghai sea dike system, but the analysis of flood consequences will not go deeper, only a comparison study with Zuid Holland and Shanghai of flood risks.

2.2 Probabilistic Analysis

Based on the new safety standard used in the Netherlands, the failure probability of a flood defence (like a dike section) has to be determined and compared to the maximum allowed probability. To assess the safety of flood defence, the failure probability of the dike section needs to be derived first, then the failure probability for every failure mechanism can be computed. Finally, a total failure probability can be calculated by combining these.

The probabilistic method can be used to calculate the failure probability. The probabilistic method needs to consider the different parameters as stochastic variables.

2.2.1 Failure Probability

The verification of safety can be performed by expressing that the load S is smaller than the structural resistance R (S. Jonkman & Schweckendiek, 2015b):

$$R > S \quad (2.1)$$

Based on this, the general form of a reliability function (limit state function (Z)) can be determined:

$$Z=R-S \quad (2.2)$$

However, resistance R and load S are not deterministic, but random variables. This means they cannot be described by one single value, but have to be described by a probability density function.

Failure occurs if the load S exceeds the resistance R , i.e. for $Z < 0$. The probability of failure is thus described by:

$$P_f = P(Z \leq 0) = P(S \geq R) \quad (2.3)$$

2.2.2 Reliability Method

There are different methods to calculate the reliability of a dike. Based on Jonkman's research, the methods can be divided into five groups: 1) Level IV, 2) Level III, 3) Level II, 4) Level I, 5) Level 0 (S. Jonkman & Schweckendiek, 2015b). In this study, the fully probabilistic methods, Level III methods are used to calculate the failure probability.

The level III methods (e.g., Monte Carlo method) are full-probability methods. The level III methods calculate the failure probability by generating stochastic numbers to model variables. Monte-Carlo simulation is a frequently used level III method, in which random samples of the parameters are generated and for each generation of samples it is determined whether failure would occur ($Z < 0$).

For the fully probabilistic calculations, fragility curves are frequent used methods to perform probabilistic calculations for dike safety assessments.

2.2.3 Fragility Curve

The first step is to estimate the probability of failure of the dike cross-section is the creation of the fragility curves. A fragility curve can express the failure probability as a function of the load and it shows the conditional failure probability for different value of loads. Moreover, fragility curves can show the influence of the load on the failure probability in a graphical way. The steeper the fragility curve, the higher the influence of the load (van Montfoort, 2018).

The following steps are followed to produce a fragility curve for a certain failure mechanism (Bischioti, 2013):

1. Define a Limit State Function (Z) for one specific failure mechanism;
2. Choose a value for the load (in this study water level);
3. Consider all other parameters, including their uncertainties and probability distributions.
4. Perform a probabilistic calculation by Monte Carlo Simulation;
5. Repeat steps 2-4 for different value of loads.

2.2.4 Numerical integration

The product of each area and the conditional probability at that water level represents the unconditional probability given a water level. By summing up all the products, the unconditional probability of one failure mode for one segment could be obtained.

Following the assumption that the strength (R) and the load (S) are independent, the failure probability for a certain value of the load, which in this study is only the water level, can be described by the integral :(van der Meer et al., 2009):

$$P_f = \int_{s=-\infty}^{s=\infty} f_{hw}(h_w) F_R(h_w) dh_w \quad (2.4)$$

in which

$f_{hw}(h_w)$ = the probability distribution function of the water level

$F_R(h_w)$ = the cumulative distribution function of the strength given a certain water level h_w

$$P_f = \sum_{i=1}^n P(f|s_i)P(s_i) = \int_0^{\infty} P(f|s_i)P(s_i)ds_i \quad (2.5)$$

in which

s_i = water level (WD)

$P(f|s_i)$ = conditional failure probability given a water level of s_i

$P(s_i)$ = probability of occurrence of s_i

2.2.5 Model Uncertainties

In this study, the uncertainties will be presented by conservative safety factors, whereas nowadays uncertainty is explicitly included as every variable is assigned a distribution. The uncertainty is expressed in the standard deviation of the variable. Model factors can be used to describe the uncertainty that will be used in this study.

Chapter 3 Failure Mechanisms and Data Analysis

To analyze the reliability of the sea dike, the first step is to identify the governing failure mechanisms. Afterward, the important data are discussed respectively.

3.1 Failure Mechanisms

Coastal flood defences like dikes react differently under the effect of hydraulic loads like waves, tides, winds, etc. Failure modes refer to the different ways that flood defences fail and failure mechanism is the process at which the flood defences are failed due to a certain failure mode. Several possible failure mechanisms for dikes are shown in Figure 3.1 (S. Jonkman & Schweckendiek, 2015b).

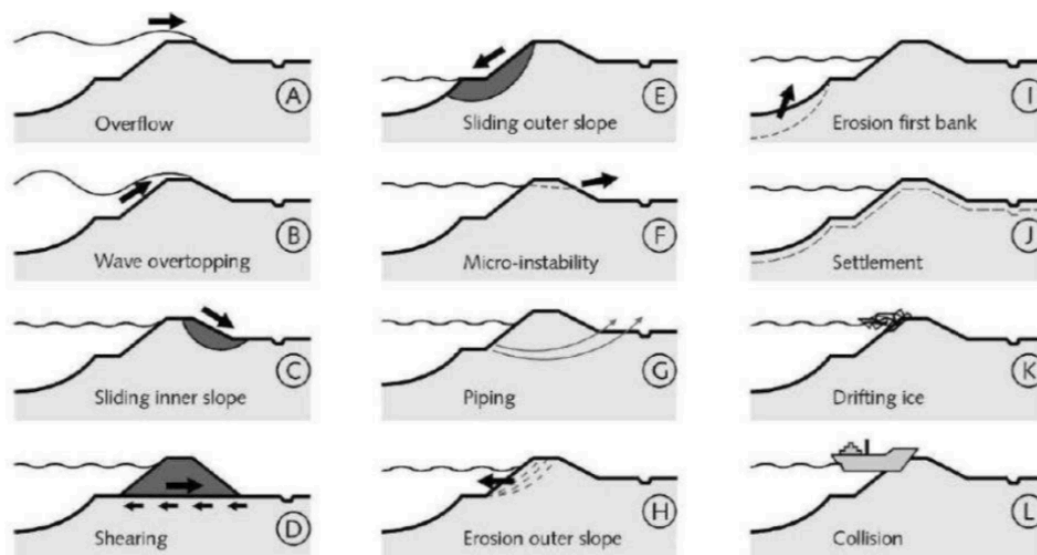


Figure 3.1: Schematic overview of the most relevant failure mechanisms of flood defences (S. Jonkman & Schweckendiek, 2015b)

These are the most common failure mechanisms for flood defences. However, only part of them is vital for sea dikes in Shanghai based on the literature reviews and some simple analyses which can be found in the following sections. Due to the workload, only the governing failure mechanisms are taken into consideration in this study. To find out the governing failure mechanisms of Shanghai sea dikes, the initial analysis of different failure mechanisms is in the next sections.

3.1.1 Overtopping/overflow

Overtopping/overflow has always been a threat to Shanghai sea dikes. Although due to the reconstruction and heightening, the overtopping/overflow rarely occurred after the 1990s.

However, according to the historical events threats of overtopping and overflow still exist. Therefore, overtopping was included in this study.

3.1.2 Macro-instability

As stated before, Cai did the analysis of the macro-instability of Shanghai sea dikes and based on his results, the safety level of this failure mechanism is not enough, so this failure mechanism will be included in this study. Macro-instability failure can occur due to the sliding of outer slopes or inner slopes and the shearing, which will be discussed respectively.

1) Sliding inner slope

The stability of the inner slope can be regarded with a classical slip circle approach. The sliding of the slope towards the protected area may occur, when the inner slope of a dike becomes unstable as a result of an increased outside water level and the water level inside the dike body. Therefore, this failure mechanism will be considered.

2) Sliding outer slope

The main trigger of this case is quick dropping of the outside water level. In this study, the quick drop water level condition is outside the research scope. However, the sliding outer slope may happen under high water condition, so this will also be included in this study.

3) Shearing

This is a typical problem for canal dikes, which have a relatively small freeboard (i.e. water level close to the crest)(S. Jonkman & Schweckendiek, 2015b). The freeboard of Shanghai sea-dikes is around 4 m in this study. Moreover, properly designed sea dikes have such a wide base (around 90 meters for Shanghai sea dikes) that horizontal sliding can usually be neglected. This problem aggravates periods of long drought, when the pore water evaporates from the dike body and the weight decreases even further. Since the phenomenon typically occurs for river dikes in winter, it is not included in this study. Moreover, the result of the deterministic calculation of this problem (in Appendix A) shows that the shearing is not a leading failure mechanism.

3.1.3 Micro-instability

With the increase of phreatic surface micro-instability occurs. The inner slope layer will be push off with the pressure in the dike body increase. Take one typical cross-section in Shanghai sea dikes as an example, the phreatic line can be simplified as depicted by numerical modelling software Seep/w and the result is shown in Figure 3.2.

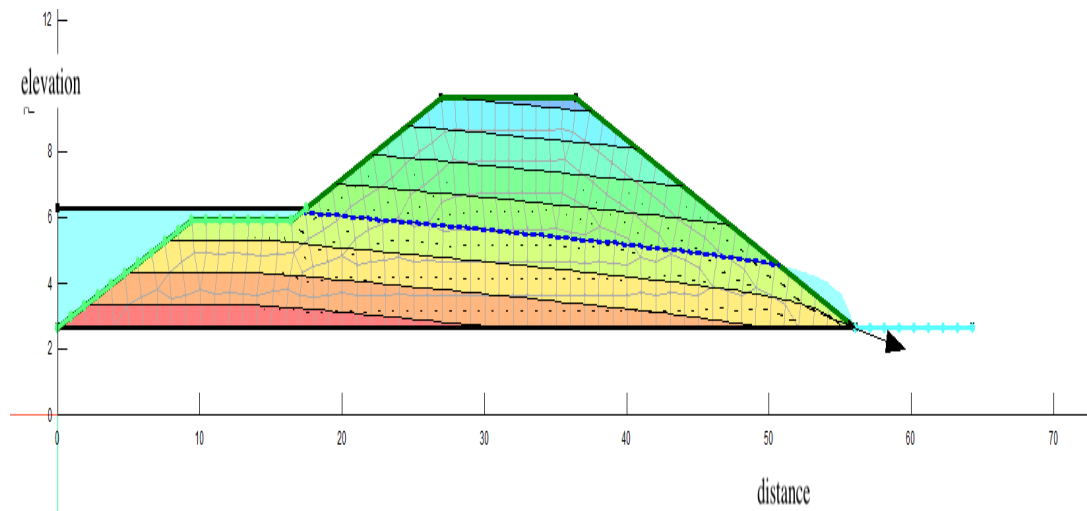


Figure 3.2: Example of phreatic line

The fact is that phreatic line at the inner slope toe is low, and due to the toe drain system (which is not considered in the upward model) the real phreatic line will be even lower, which means micro-instability hardly will happen, so this failure mechanism will not be included in this study.

3.1.4 Piping

Piping occurs under the dike due to the erosive action of seepage flow which causes the continuous transport of soil particles(S. Jonkman & Schweckendiek, 2015b). Since the soil under the Shanghai sea-dikes is mainly clay instead of sand, together with the deterministic in Appendix A, so the piping will not be included in the main failure mechanisms.

3.1.5 Revetment failure (erosion of outer slope)

For coastal structures, this failure mechanism often occurs under storm condition which mainly induced by the action of waves. One previous research of the safety of Shanghai sea dikes show that the erosion of the outer slope also needs to be considered(Cui, He, & Liu, 2018). The inner slopes of Shanghai sea dikes are grass covered and the stability of inner

slope will also be influenced by the overtopping. In this study, only the outer slope instability is taken into account in Section 4.3.

3.1.6 Other Failure Mechanisms

- **Erosion of first bank**

This failure mode is a typical failure mechanism for river dikes and always occurs at dikes with a channel before it. The Figure 3.3 and Figure 3.4 show the variation of the channel in Yangtze River estuary, due to the sediment transport of Yangtze River, the channel is sedimented, which causes continuous siltation of the channel in foreshore zone(J. Zhang, Chen, Wu, & Zhao, 2015). Therefore, the first bank of Shanghai sea dikes is more likely to suffer from sedimentation instead of erosion, this failure mechanism will not be included in this study.

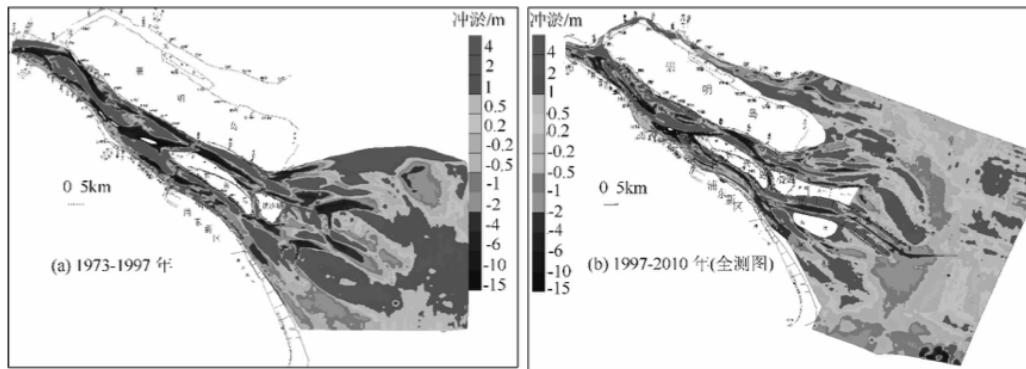


Figure 3.3: Variation of Yangtze River Estuary morphology(J. Zhang et al., 2015)

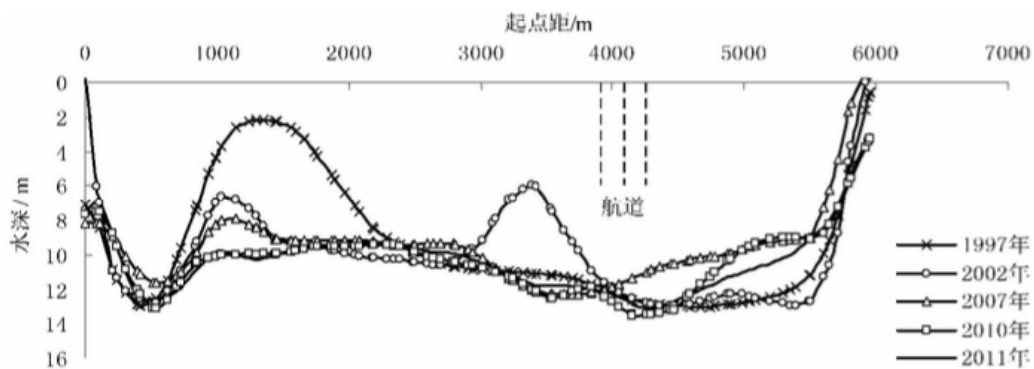


Figure 3.4: Variation of the cross-section in South Channel, Yangtze River Estuary(J. Zhang et al., 2015)

- **Settlement**

As shown in Figure 3.5 and Figure 3.6, statistics on the average value of the monitoring settlements from 2009 to 2015 show that the settlement rates are nearly normal distributed. The variation range of settlement or uplift of more than 70% of the coastline is within 20 mm/a, and the maximum settlement rate reaches 65 mm/a. The Nanhui District suffers the most severe settlement(Chen, Yong, Shi, Li, & Yu, 2016).

The soils under the Shanghai sea dikes are compressible. After construction or reinforcement dikes often settle in the order of decimeters or meters in the years and decades after completion of the works.

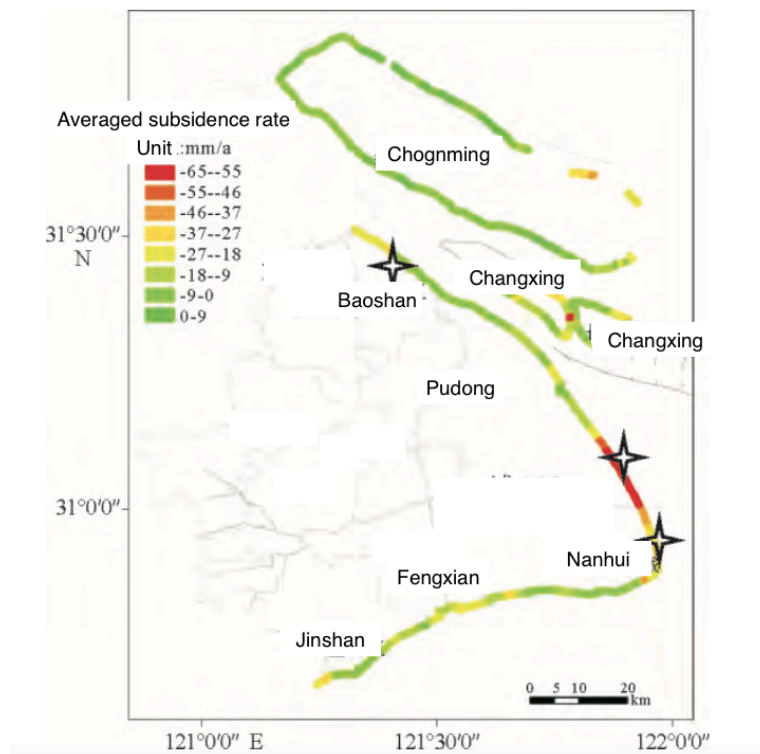


Figure 3.5: Averaged subsidence rate between 2009—2015 (Chen, Yong et al., 2016)

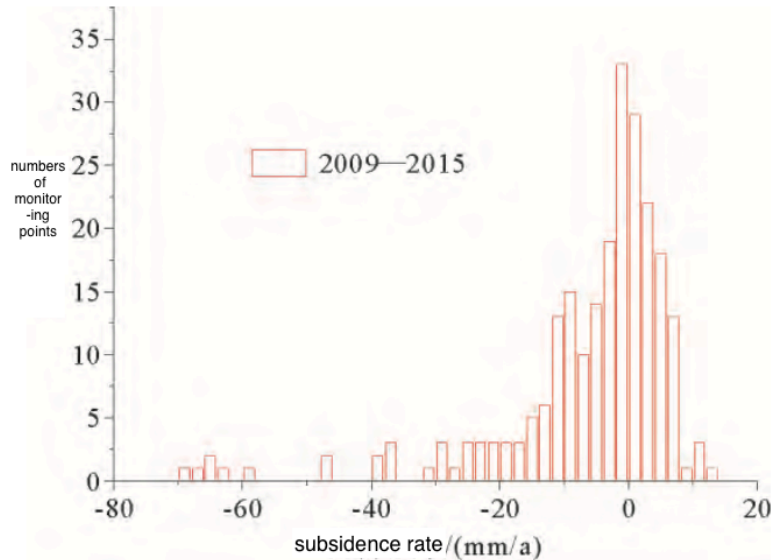


Figure 3.6: Frequency distribution diagram of Shanghai sea dike subsidence rate between 2009—2015 (Chen , Yong et al., 2016)

The land subsidence will mainly influence the crest elevation and will cause threats due to the insufficient crest height. However, the crest elevation used in this study was measured last year, so the effect of subsidence has been taken into account, and this study only focus on existing failure probability, so the land subsidence will not be included in this study. For assessment of future conditions, this will also need to be considered.

- **Drifting ice**

Due to the location of Shanghai (30°N) and the average temperature in winter(3~5°C) (Shanghai Municipal Bureau of Statistics, 2018), the drifting ice is not a threat to the sea dikes. Therefore, this problem will not be included in this study.

- **Collision**

Though collision of a vessel with a dike is a theoretical possibility, it is seldom considered as a failure mechanism in the design and assessment of dikes. The mechanism is more relevant for hydraulic structures like locks and sluices. Therefore, this problem will not be included in this study.

3.1.7 Summary

To summarize, the sea dikes in Shanghai are mainly under the following threats and these failure mechanisms will be discussed in this study respectively and this will not include the effects of typhoons which is out of the scope of this study, so in this study the typhoons will not be taken into account when considering the high water level. Other failure mechanisms

may also cause floods, but they are not the governing failure reason for Shanghai sea dikes, so these are not further described here.

In this study, the critical failure mechanisms are:

- 1) Overtopping
- 2) Revetment instability
- 3) Macro-instability (sliding of inner and outer slope)

3.2 Data Analysis

As stated in the previous sections, the main failure mechanisms of Shanghai sea dikes are overtopping, revetment instability and macro-instability. To calculate the failure probability of each failure mechanism, the boundary conditions need to be introduced. The boundary conditions are initial data of the load and resistance parameters which are used in the limit state function. After analysis of these data, the distribution of variables can be derived to perform reliability analysis.

Based on the characteristics of the three failure mechanisms, there are three types of boundary conditions essential, which are hydraulic boundary conditions, structural boundary conditions and geotechnical boundary conditions. These boundary conditions are important for the section divisions and failure probability calculations in the next sections.

3.2.1 Hydraulic Boundary Conditions

Hydraulic boundary conditions include water level, wave, wind, etc. information, which are the essential load parameters for the three target failure mechanisms in this study.

(1) Water level

High water level is a big threat to the safety of Shanghai sea dikes. There are mainly two interrelated factors that can increase sea water level of Shanghai: namely astronomic tide, storm surge.

- **Astronomic tide**

In general, the sea water level is determined by the astronomic tide which represents periodic rise and fall of sea level due to differential attraction of sun and moon(S. Jonkman & Schweckendiek, 2015b). The tidal range is the vertical difference between the high water and the low water, which changes from cycle to cycle and the period of tide is usually 12 hours

(semi-diurnal tide). Tides are very predictable and low uncertainties rates. The historical highest astronomic tide and its average value at Wusongkou¹ are 4.63m (WD²) and 3.51m, respectively(Ke, 2014).

- **Storm surge**

Storm surge is a largescale increase in sea level generated by a storm, over and above the predicted astronomical tides(S. Jonkman & Schweckendiek, 2015b). This increase in water level can cause flooding in coastal areas particularly when storm surge coincides with normal high tide. This water level increases due to the combination of the astronomical tide and storm surge is defined as the storm tide. In this study the effect of typhoon will not be included.

As for Shanghai sea dikes, the water level information was adopted from the conclusion made by Shanghai Water Authority. The water level data were collected from five hydrological stations located along the Shanghai coastline, respectively (See Figure 3.7): Wusongkou, Gaoqiao, Sanjiagang, Luchaogang and Jinshan. The Shanghai Water Authority conducted the water level with various return periods based on the flood probability analysis in the last decade, and the results are shown in Table 3.1. Based on the information provided by Shanghai Water Authority, the annual maxima long-term water levels and the Pearson type III distribution with a curve fitting method are used in this frequency analysis. Since the longtime data of water level are collected from the tide gauges, so the water level includes the astronomic tide, storm surge, sea level rise, so the water levels in the Table 3.1 are the combinations of these factors.

¹ Hydrological station whose location is introduced in Figure 3.1

² Hereafter, water levels and geographic elevations are referred to Wusong Datum (WD). WD is 1.924m lower than mean sea level of China Yellow sea; the mean sea level of Yellow Sea is a reference datum for China in general, while local datum is applied widely in China, e.g. WD.

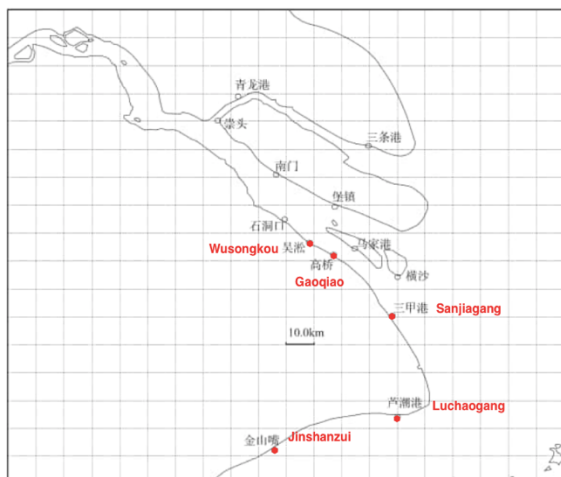


Figure 3.7: Locations of hydrological stations along Shanghai coastline: Wusongkou, Gaoqiao, Sanjiagang, Luchaogang and Jinshanzui. (Shanghai Water Engineering design and Research Institute, 2012)

Table 3.1: Water level for different return periods [WD].

No.	Tide gauge	Return period						
		1000	500	200	100	50	20	10
1	Wusongkou	6.6	6.44	6.21	6.04	5.87	5.63	5.44
2	Gaoqiao	6.94	6.73	6.43	6.21	5.98	5.68	5.44
3	Sanjiagang	6.82	6.6	6.3	6.07	5.83	5.52	5.27
4	Luchaogang	6.42	6.24	5.99	5.8	5.62	5.37	5.18
5	Jinshanzui	7.34	7.13	6.83	6.6	6.37	6.06	5.82

The magnitude of flood events is inversely proportional to their occurrence frequency. The relation between the return periods and the corresponding water levels is a statistic description of water level. The frequency analysis of hydrologic data can relate the magnitude of extreme events to their frequency of occurrence by using probability distributions (Van Westen, Alkema, Damen, Kerle, & Kingma, 2011). The distribution characteristics of random variables can be determined mathematically based on the historical observed data. Therefore, the frequency curves of water level would be derived by the hypothesized PDF or CDF is fitted to the data.

However, the exact probability distribution functions are not given by the Shanghai Water Authority. To make a flood frequency analysis, it is necessary to compare the assumed population with the sample data. In general, the sample values are plotted in a figure by assigning each of them an exceed probability based on the plotting position formula (Gringorten, 1963). The annual maximum water levels used for frequency analysis of different tide stations were collected from 1998 to 2015.

As stated before, the Shanghai Water Authority chose Pearson-III distribution to describe the water level data, so the same distribution is used in this study for water level conditions.

- **Pearson-III Distribution**

Followed by the “Chinese standards of design flood calculation in hydraulic engineering”, the frequency distributions of hydrological stochastic variables are adopted as Pearson Type III in general. The Pearson Type III distribution is shown as below:

$$F(x) = P(x \geq x_p) = \frac{\beta^\alpha}{\Gamma(\alpha)} \int_{x_p}^{\infty} (x - a_0)^{\alpha-1} e^{-\beta(x-a_0)} dx \quad (3.1)$$

$$a_0 = E(X) \left(1 - \frac{2C_v}{C_s}\right) \quad (3.2)$$

$$\alpha = \frac{4}{C_s^2} \quad (3.3)$$

$$\beta = \frac{2}{E(x)C_v C_s} \quad (3.4)$$

Where: $E(X)$ is mean value; C_v is kurtosis; C_s is skewness.

If the parameters of $E(X)$, C_v , C_s can be determined the probability density function of water level along Shanghai coastline can be deduced. Since the dataset only includes 17 years, the results of Shanghai Water Authority are also used to give a better curve fit. Figure 3.8 shows an example of a curve fitting of Wusongkou, and Table 3.2 gives the result of probability analysis. The ‘probability’ in Figure 3.8 means the probability that the water level exceeds the specific value.

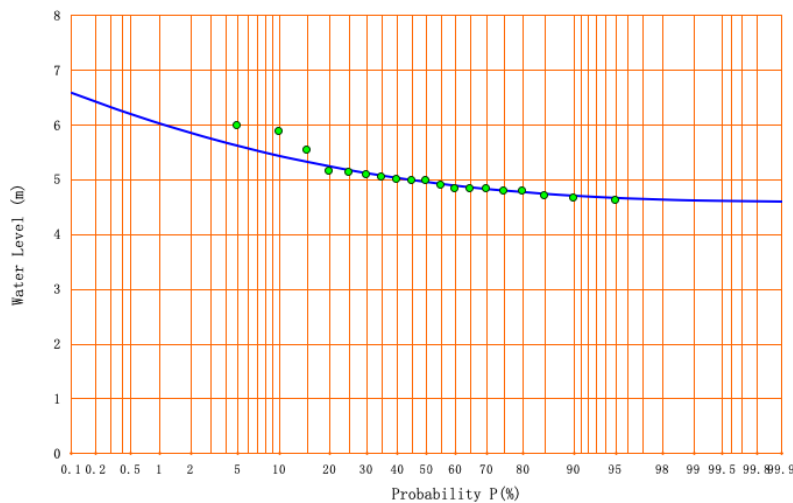


Figure 3.8: Fitting curve of Wusongkou

Table 3.2: Results of water level frequency analysis

Tide Station	Distribution	Parameter		
		α [-]	β [-]	a_0 [-]
Wusongkou	P-III	2.03	4.64	4.82
Gaoqiao	P-III	1.02	3.16	4.90
Sanjiagang	P-III	1.24	3.45	4.95
Luchaogang	P-III	2.11	5.04	5.22
Jinshanzui	P-III	1.23	2.78	5.10

Wave characteristics are also important for the main three failure mechanisms. However, due to the insufficient information of the wave data of Shanghai, the wind data are used to simulate the wave condition in Shanghai.

(2) Wind

According to the comparison of the longtime series data of Xuhui, Minhang meteorological stations with the data from the pilot ship, the correlation between the inland and coastal wind speed can be derived by Shanghai Water Authority. The locations of meteorological stations are shown in Figure 3.9. The basic information including meteorological stations, the periods and type of wind dataset are summarized in Table 3.3(*Code for Design of Levee Project*). Using this result, the daily maximum wind speed data of five districts can be transformed to the coastal daily maximum wind speed data, then the frequency analysis was conducted which gives the coastal wind speed of different directions with various return periods of five different parts along the Shanghai coastline (Baoshan, Pudong, Nanhui, Fengxian and Jinshan), the wind characteristics of Baoshan are shown in Table 3.4 as an example(*Code for Design of Levee Project*).

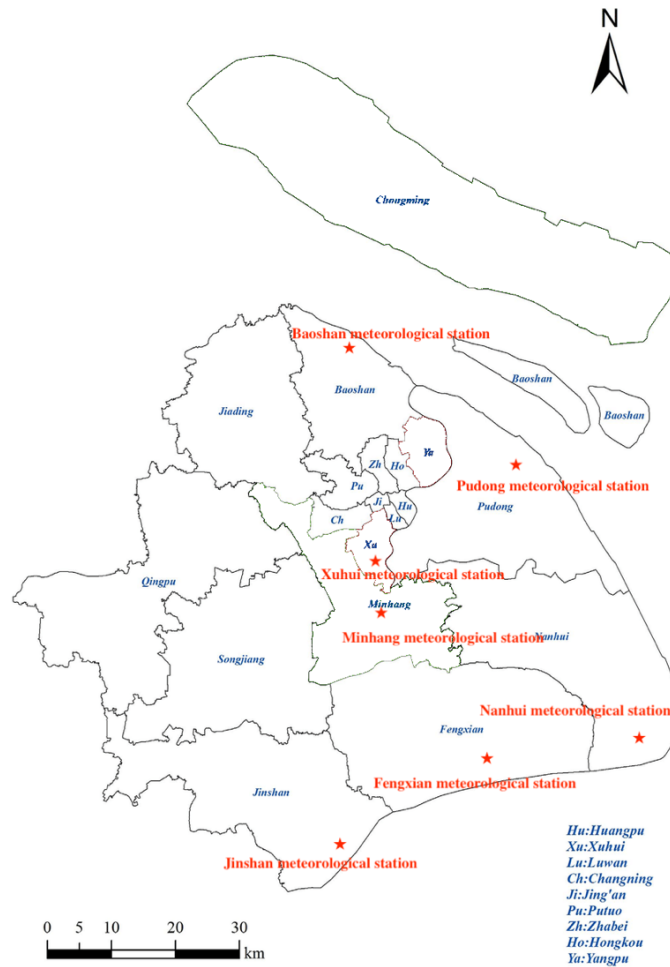


Figure 3.9: Locations of meteorological stations.

Table 3.3: Basic information of wind dataset. (Code for Design of Levee Project).

Meteorological stations	Datasets periods	Type
Baoshan	1974-01 to 2010-03	daily maximum wind speed
Nanhui	1974-01 to 2010-03	daily maximum wind speed
Fengxian	1974-01 to 2010-03	daily maximum wind speed
Jinshan	1974-01 to 2010-03	daily maximum wind speed
Chongming	1974-01 to 2010-03	daily maximum wind speed
Xuhui	1901 to 1970	Series data
Minhang	1971 to 2009	Series data

Table 3.4: Wind characteristics of Baoshan part (Code for Design of Levee Project).

direction	N	NE	E	SE	S	SW	W	NW
Return period[yr]	[m/s]							

5	19.1	19.2	19.1	17.3	16.2	16.8	18.3	18.3
10	21.7	21.7	21.5	19.3	18.9	18.9	20.4	20.6
20	24.3	24.1	23.8	21.3	20.8	20.8	22.5	22.8
50	27.5	27.1	26.7	23.7	23.3	23.3	25.1	25.5
100	30.0	29.3	28.9	25.6	25.1	25.1	27.0	27.6
200	32.5	31.7	31.2	27.5	27.0	27.0	29.1	29.7
300	33.8	33.0	32.4	28.5	28.1	28.1	30.2	30.9
500	35.8	34.8	34.1	30.0	29.6	29.6	31.8	32.5
1000	38.2	37.0	36.3	31.8	31.4	31.4	33.7	34.6

Since the known data of wind characteristics are of the frequency of occurrence of the wind speeds which are shown by means of a return period, the exceedance probability and the cumulative probability are known. However, the exact distribution characteristics are unknown and the basic data of wind characteristics data are insufficient. Therefore, instead of normal frequency analysis which using the sample values to plot in a figure by assigning each of them an exceed probability based on the plotting position formula and fitting the results with the probability density functions of different distributions, this study will use the cumulative probability function to fit the existing wind frequency data.

Different regions or countries adopt an appropriate probability distribution differently, for example, the log Pearson type III (the US) and the general extreme value (GEV) distribution (the UK), and the Pearson type III distribution (China). Based on the characteristics of the datasets, three probability distributions were selected to analyze the frequency of wind speed, namely Pearson-III, Gumbel and Weibull distribution.

Using the wind speed data of Northwind in Baoshan part as an example, the results of fitting curves in P-III, Gumbel, and Weibull distribution are shown in Figure 3.10.

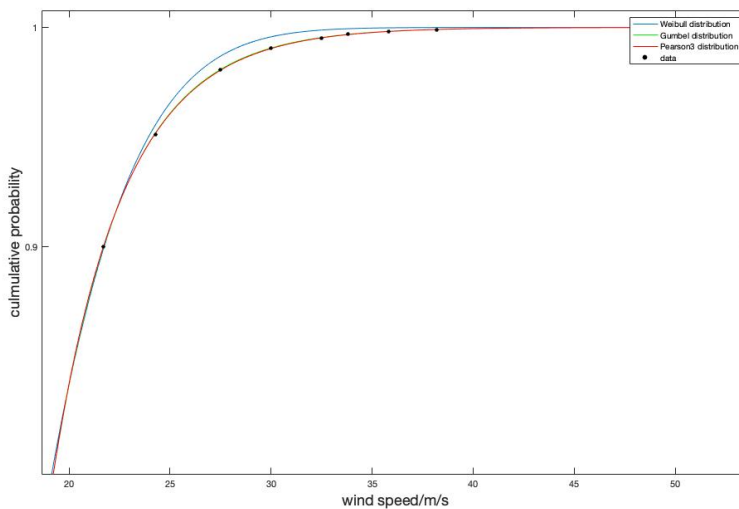


Figure 3.10 :Fitting curves of wind speed (N, Baoshan)

To select the appropriate distribution, two estimation methods, the R-Square (COD), Residual Sum of Squares (RSS) (Reduced Chi-Sqr) are taken into account.

a) Coefficient of determination

R-square (COD) is a statistical measure to qualify the linear regression. Hence, R-square is always between 0 and 1. In general, the larger the R-square, the better the fitted line fits the data.

b) Residual Sum of Squares

RSS is the sum of the square of the vertical deviations from each data point to the fitting regression line. In general, the smaller the residual sum of squares, the better the model fits your data.

In short, the larger the COD is and the smaller the RSS is, the distribution is a statistically better fit. In Table 3.5, the three distributions all show good fit results than P-III distribution. Considering the P-III distribution is recommended to describe the wind speed in the Technical regulations for seawall engineering in Zhejiang Province (which is next to Shanghai), the P-III distribution is recommended as the probability distribution for datasets of the wind speed.

Table 3.5: Results of statistical performance indicator

Probability distribution		P-III		Gumbel		Weibull	
Sub-division	Wind direction	COD	RSS	COD	RSS	COD	RSS
Baoshan	N	1	8.16E-8	1	1.09E-6	0.99995	4.6E-5

According to the fitting curve figure and the value of COD and RSS, it can be seen that the P-III and Gumbel distributions give a better fit than the Weibull distribution. To make sure which distribution is best for the wind speed, the design wind speed needs to be taken into account. Since the Shanghai sea dike is designed under the 200-year return period (cumulative probability=0.995) of wind speed (32.5m/s for N direction at Baoshan part), which distribution that gives the best fit on this point needs to be figured out. The P-III gives an exact fit on the design point (cumulative probability=0.995 when wind speed=32.5m/s). Therefore, the P-III distribution is chosen to describe the wind speed and the P-III parameters of different parts and wind directions can be deduced, the results are shown in Table 3.6:

Table 3.6: Results of probability analysis of wind speed

Sub-division	Wind direction	P-III parameters		
		α [-]	β [-]	a_0 [-]
Baoshan	N	1.44	3.32	11.20
	NE	2.01	2.79	10.82

	NW	1.77	2.8	11.56
Pudong	N	1.79	3.73	10.27
	NE	1.55	4.07	11.15
	E	2.38	2.7	10.45
Nanhui	N	1.79	3.73	10.27
	NE	1.55	4.07	11.15
	E	2.38	2.64	11.69
	SE	1.86	2.32	9.2
	S	1.41	3.32	10.9
	SW	1.62	3.28	8.35
Fengxian	SE	1.54	2.69	12.72
	S	2	2.12	10.55
	SW	1.56	2.71	9.48
	E	1.58	2.82	11.63
Jinshan	SE	1.91	2.73	10.37
	S	1.63	2.91	9.53
	SW	1.81	2.66	8.41
	E	2.4	2.7	9.63

(3) Wind Wave

Wind waves coupled with high water levels can pose threats to the flood defence. There is little direct measured wave information available, the empirical formulas were considered to estimate the wave height along Shanghai coastline. The wind wave mainly depends on the wind speed, the length of the wind zone and the water depth.

The formulas were adopted to calculate the wind waves along the Shanghai coast (Ministry of Water Resources, 2014):

$$\frac{g\bar{H}}{U^2} = 0.13 \tanh \left[0.7 \left(\frac{gd}{U^2} \right)^{0.7} \right] \tanh \left\{ \frac{0.0018 \left(\frac{gF}{U^2} \right)^{0.45}}{0.13 \tanh \left[0.7 \left(\frac{gd}{U^2} \right)^{0.7} \right]} \right\} \quad (3.5)$$

$$\frac{g\bar{T}}{U} = 13.9 \left(\frac{g\bar{H}}{U^2} \right)^{0.5} \quad (3.6)$$

$$H_s \approx H_{13\%} = \bar{H} \left[-\frac{4}{\pi} \left(1 + \frac{1}{\sqrt{2\pi}} H^* \right) \ln 13 \right]^{\frac{1-H^*}{2}} \quad (3.7)$$

$$T_p = 1.21 \bar{T} \quad (3.8)$$

in which

\bar{H} = average wave height (m)

H_s = significant wave height (m)
 $H^* = \bar{H}/d$, relative water depth
 d = average water depth (m)
 U = wind speed at 10m high (m/s)
 F = fetch (m)
 \bar{T} = average wave period (s)
 T_p = peak wave period (s)
 g = gravitational acceleration (m/s²)

To utilize the formulas, data of fetch and average water depth were necessary. According to *Computation and Verification of Wave Characteristics along the Coastal Water of Yangtze River Estuary and Hangzhou Bay*, the fetch and average water depth of different directions are shown in the Table 3.7 The distance along the sea dike alignment is measured from the NW end.

Table 3.7: The fetch and corresponding average water depth(Qiyi & Guangwen, 1994)

Distance along the sea dike alignment	0km-32km			32km-56km				
Wind direction	N	NE	E	N	NE	E	NW	-
Fetch[km]	15	15	15	7	6	11	30	-
Average water depth[m]	10	10	10	13	15	15	14	-
Distance along the sea dike alignment	56km-90km				90km-116km			
Wind direction	N	NE	E	NW	N	NE	E	SE
Fetch[km]	150	6	11	30	150	6	11	30
Average water depth[m]	17.5	15.5	15	14	17.5	15.5	15	14
Distance along the sea dike alignment	116km-138km				138km-210km			
Wind direction	S	SW	E	SE	S	SW	E	SE
Fetch[km]	150	6	11	30	47	48	110	100
Average water depth[m]	17.5	15.5	15	14	17.5	17.5	17.5	17.5

The wave data at the toe of the dikes can be obtained by transferring the significant wave height, this was predicted by using wind data, from offshore to the position of the toe, taking into account shoaling, refraction and breaking. The whole process is shown in Figure 3.11:

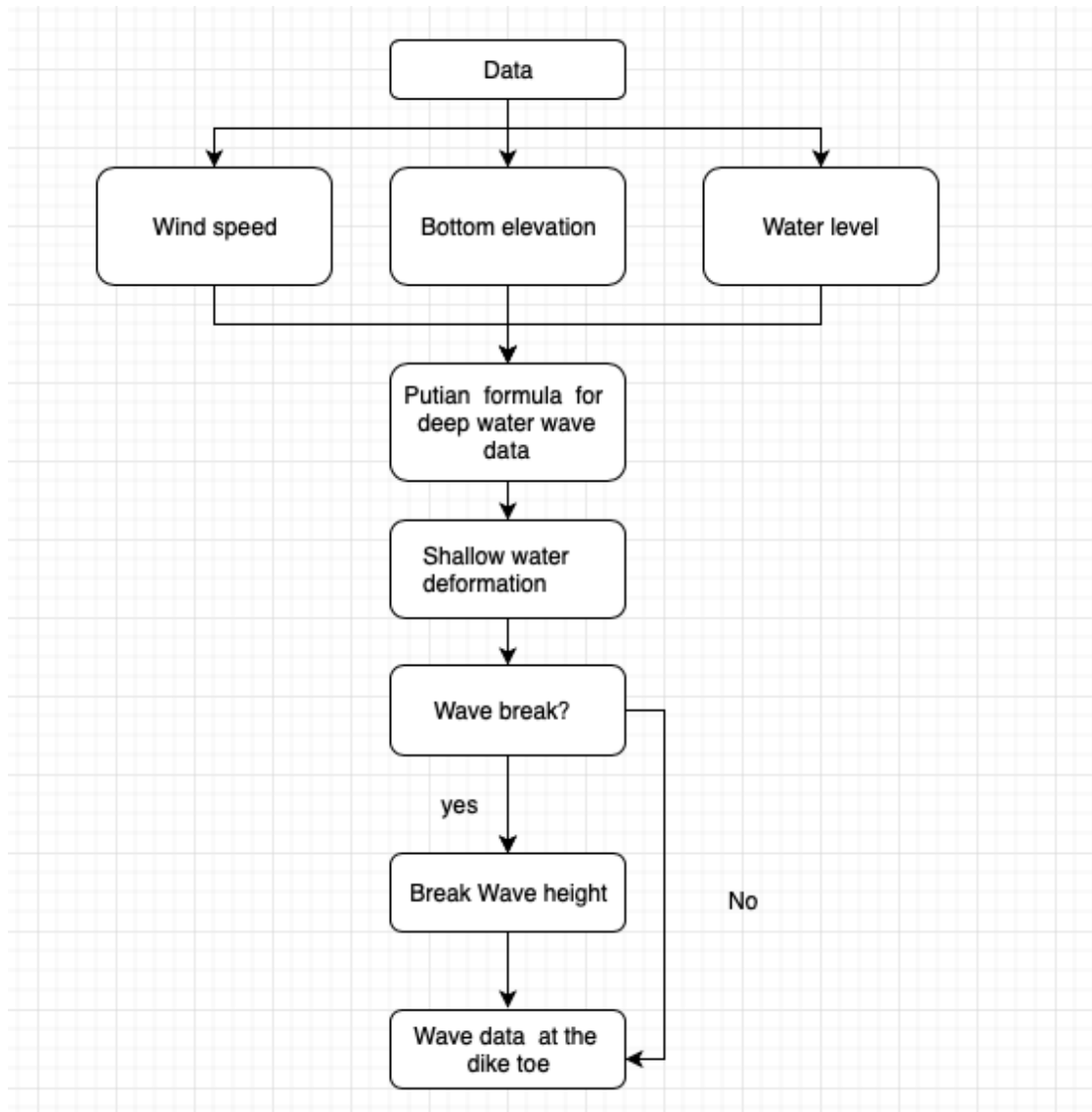


Figure 3.11: Process of wave deformation calculation.

3.2.2 Structural Boundary Conditions

(1) Crest elevation

The crest elevation data are the measurement result from the fieldwork in Shanghai in September 2019. Since only the crest elevation and the crown wall elevation have been measured for 104 points along the coast, several assumptions are made for the actual situation: (Yin, 2020b)

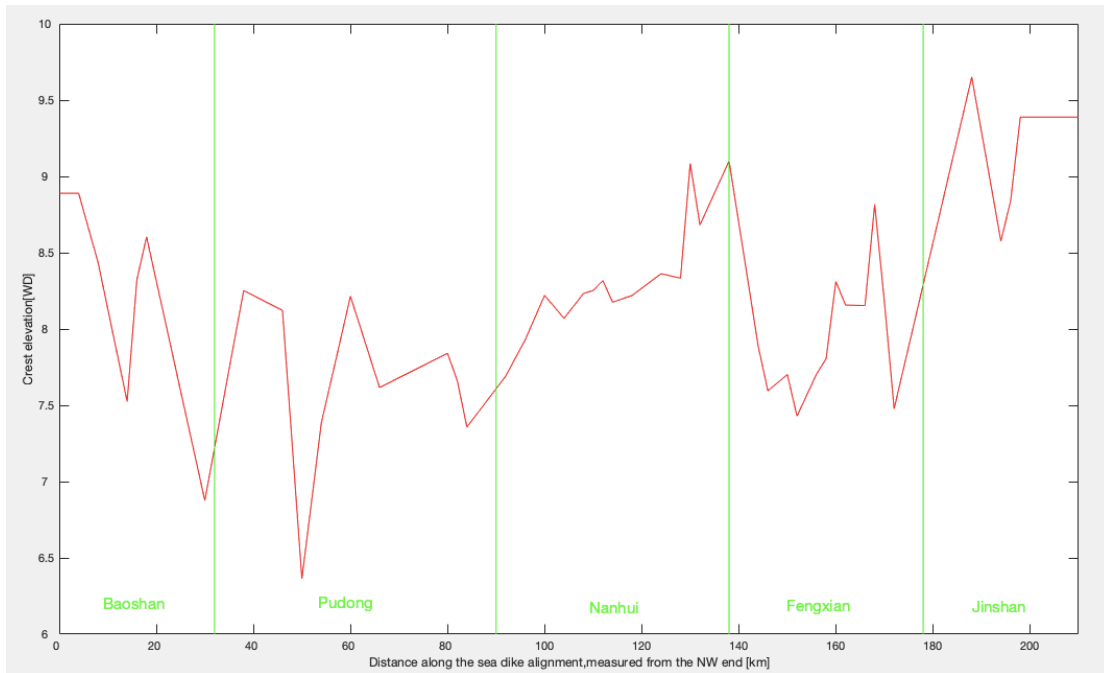


Figure 3.12: Crest elevation of Shanghai sea dikes

(2) Geometry

The typical cross-section of the Shanghai sea dike is shown in Figure 3.13 and the detailed cross-sections of different sub-divisions are stated in following. The important data are summarized in Table 3.8. h_{crest} =crest elevation + crown wall height.

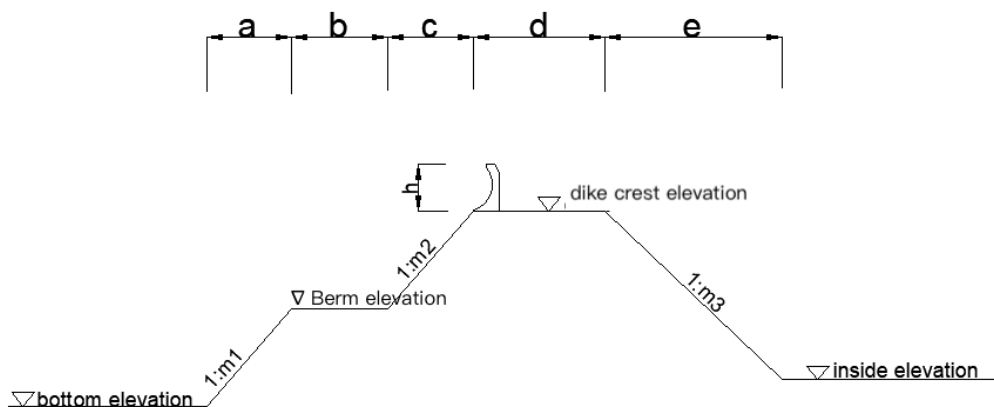


Figure 3.13: Typical cross-section of Shanghai sea dikes

Table 3.8: Cross-section characteristics

Sub-division	h_crest [WD]			Slope			Inside elevation [WD]
	Dike Crest elevation [WD]	H[m]		m1	m2	m3	
Baoshan	Figure 3.12	1.2		3	3	3	4.5
Pudong							4.6
Nanhui							4.5
Fengxian							4.4
Jinshan							4.5
Sub-division	a [m]	b[m]	c[m]	d[m]	e[m]	Berm elevation [WD]	Bottom elevation [WD]
Baoshan	9	5	6	9.5	9	5.6	1
Pudong	9	7	9.75	9.5	14.1	5.9	2.5
Nanhui	7.5	5	7.95	9.5	12	5.5	2.5-2.75
Fengxian	5	4.5	7	8	10.35	5.5	1
Jinshan	10.5	6	9	10	13.5	6	1

(3) Orientation

The orientation of the flood defence is an important parameter for overtopping. To simplify the calculation, the whole sea dike system can be divided into eight parts based on the orientation of the sea dike, which is shown in Figure 3.14. The details of this division are listed in Table 3.9. The “orientation” in Table 3.9 stands for the orientation angle of the normal line of the Shanghai sea dikes.

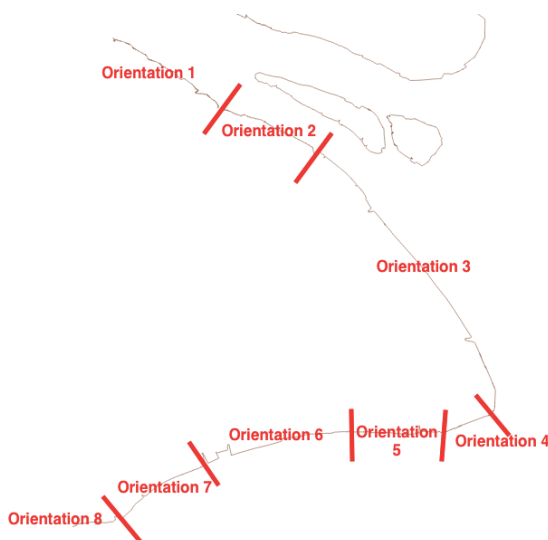


Figure 3.14: Orientation of Shanghai sea dikes

Table 3.9: Orientation division(“orientation” in Table 3.9 stands for the orientation angle of the normal line of the Shanghai sea dikes.)

Distance along the sea dike alignment	0km-32km	32km-46km	46km-116km	116km-126km	126km-146km	146km-178km	178km-198km	198km-210km
Orientation[°]	31	24	58	153	180	162	125	164

3.2.3 Geotechnical Boundary Conditions

(1) Soil Properties

Cai Xiaofang divided the Shanghai sea dikes into two parts, Southside of the Yangtze River (Baoshan district, Pudong district and Nanhui district) and Northside of Hangzhou Bay (Fengxian district and Jinshan district), and collected the soil property of the two parts shown in Table 3.10 and Table 3.11(Cai, 2017). Based on previous researches on regarding the soil properties, Cai assumed that most soil characteristics follow the normal distribution(Minoru, 1990) and the standard deviations are also shown in the Tables. According to the data, the typical soil layers under the Shanghai sea dikes are soft clay which has relatively larger natural water content, void ratio and compressibility but lower shear strength(W. Wang, Xu, & Li, 2018).

Table 3.10: soil property of South side of the Yangtze River(Cai, 2017)

Numbers	Name	Thickness(m)	γ (kN/m ³)		C(kPa)		Φ (°)	
			μ	σ	μ	σ	μ	σ
1	Fill	1.1	18.2	0.08	7	2.65	29.5	3.81
2	Muddy Silty clay	2.2	17.1	0.04	101	1.57	20.5	2.18
3	sandy clay	2.6	18.5	0.04	13	2.73	33	2.25
4	Muddy silty clay	3.2	17.0	0.04	11	1.98	18.5	4.07
5	Muddy ay	11.3	16.3	0.03	10	1.38	11.5	1.7
6	clay	-	17.3	0.04	13	1.82	14.5	1.93

Table 3.11: soil property of North side of Hangzhou Bay(Cai, 2017)

Numbers	Name	Thickness(m)	γ (kN/m ³)		C(kPa)		Φ (°)	
			μ	σ	μ	σ	μ	σ
1	Silt	0.15	16	-	5	-	2	-
2	Silty clay	1.3	18.7	0.04	12	3.01	27.5	4.86
3	Sandy clay	10	19.5	0.08	7	5.1	27.5	6.98
4	Muddy clay	10.3	16.5	0.03	14	0.59	10.5	1.54

Chapter 4 Conditional Failure Probability

To get the conditional failure probability, the first step is to divide the whole dike system into small sections with homogeneous properties. Then, based on the characteristics of three main failure mechanisms, the limit state function and the parameters can be derived. After that, the conditional failure probability at the section level of each failure mechanism can be calculated.

4.1 Section Decomposition

As stated before, the new safety standards have come into force in the Netherlands at the beginning of 2017. The standards are determined by a *dike trajectory* instead of a dike ring (which is used for the old safety standards). A part of a dike ring that has the same consequences is a dike trajectory. To assess the reliability of Shanghai sea dikes, a similar approach can be used in this study. Considering the failure of Shanghai sea dikes will cause the same threat to this metropolis, the Shanghai sea dike system can be seen as a dike trajectory.

To calculate the total failure probability of the Shanghai sea dike system, the Shanghai dike trajectory which is shown in Figure 1.2 can be split up into multiple sections. For each dike section and each failure mechanism, the failure probability is calculated. Furthermore, combining the failure probabilities of the different sections, taking into account the *length effect* for every failure mechanism can give an insight of the system failure probability of Shanghai sea dikes. The *length effect* will be discussed in the later section.

4.1.1 Sub-division

As stated before, the whole Shanghai sea-dikes system can be divided into five parts, named Baoshan, Pudong, Nanhui, Fengxian, and Jinshan respectively, based on the Shanghai districts and the difference of the cross-sections, which are shown in Figure 1.2.

4.1.2 Sub-division decomposition

The Shanghai sea dike system consisted of different types of dike cross-sections, and the strength and load conditions varied, so the sub-division had to be divided into smaller sections. The principle was that within each section the properties of strength and load properties can be assumed to be homogeneous.

Since many parameters are affecting the section division, the first step is to determine the predominant parameters, which is accomplished by determining which failure mechanism is the most influential according to the calculated failure probability. This is an iterative

procedure because the most influential failure mechanism could not be determined without failure probability calculations stated in the latter.

Overtopping/overflow is considered as the most influential failure mechanism based on the results of failure probability calculation, which are shown in Table 5.2. Correspondingly, based on the relevant variables, like crest level, water level, wave conditions (including wind speed, wind direction, fetch, and water depth), and structure orientation, the sub-division can be further divided into small sections.

The water level data were analyzed in Section 3.2.1, where data is available at only five locations (historical measurement stations), shown in Figure 3.7. To see the locations of these points more clearly and directly, the distances of these stations along the sea dike alignment, measured from the NW end, are shown in Figure 4.1 (red five-pointed stars).

The five water level data points can describe the water level data near them. For instance, the water level data of the Jinshan sub-division can be assumed to be the data of water level 5. However, some analysis needed to be done to make sure the exact part that each water level data point can represent. The data used for validation are the total water level recorded every hour from 15 August to 21 August in 1997, which is provided by Shanghai Water Authority, and the simulation water level data by Delft3D (Figure 4.1) (Yin, 2020b).

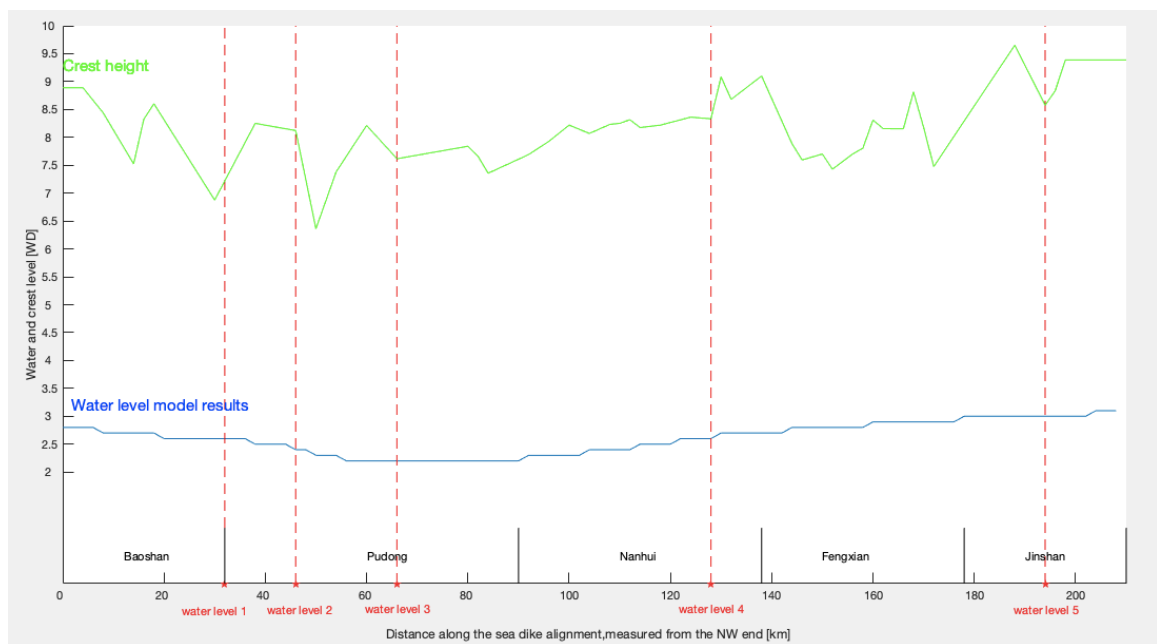


Figure 4.1: Max. Water level data from 15 August to 21 August in 1997

In Figure 4.1:

- The red five-pointed stars and red dotted line represent the locations of historical measurement stations (water level data);

- The blue line represents the model results of water level from Delf3D;
- The black line represents the dike sub-divisions based on Shanghai districts;
- The green line shows the dike crest elevation.

From Figure 4.1, the water level condition can be roughly divided into several parts. For example, the water level condition of Baoshan sub-division can be assumed to be the water level 1 and the water level condition of Jinshan sub-division can be assumed to be the water level 5 at first. As for the other three sub-divisions and the detailed boundary that each water level data point can be applied to need more analysis.

By using the hourly recorded water level data, the difference in water level varying between different locations can be seen. For example, by comparing the water level data of $x=0$ Km, $x=16$ Km, $x=32$ Km (Water level point 1), the varying of the water level at the three locations are similar which are shown in Figure 4.2, so it can be assumed that the water level 1 can be used to represent the water level condition from $x=0$ Km to $x=32$ Km (Baoshan sub-division). Moreover, by comparing the water level data of $x=38$ Km, $x=32$ Km (Water level point 1) and $x=46$ Km (Water level point 2) in Figure 4.3, the red line is closer to the blue line which means from $x=40$ km the Water level point 2 gives a better description of water level, so the water level 1 can represent the water level from $x=0$ Km to $X=38$ Km.

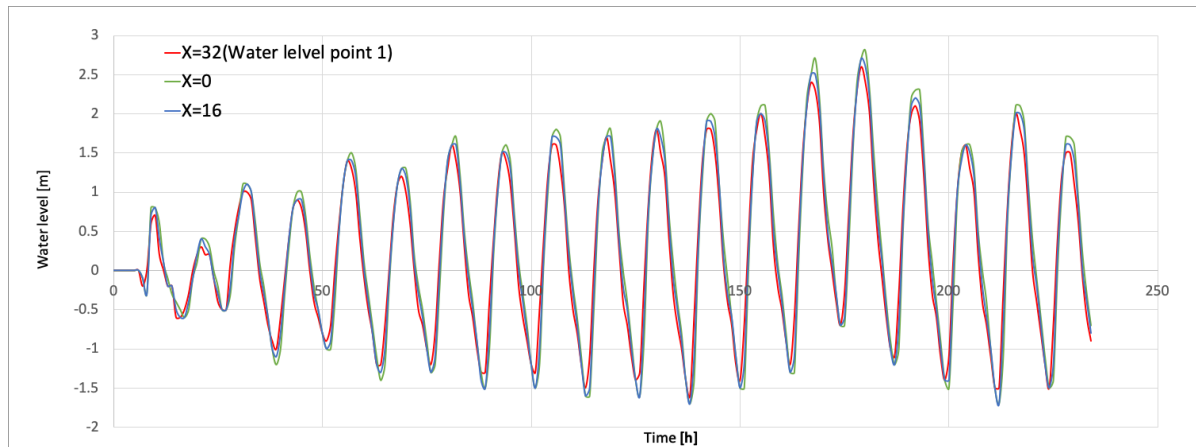


Figure 4.2: Water level variation of three locations ($x=0,16,32$ km)

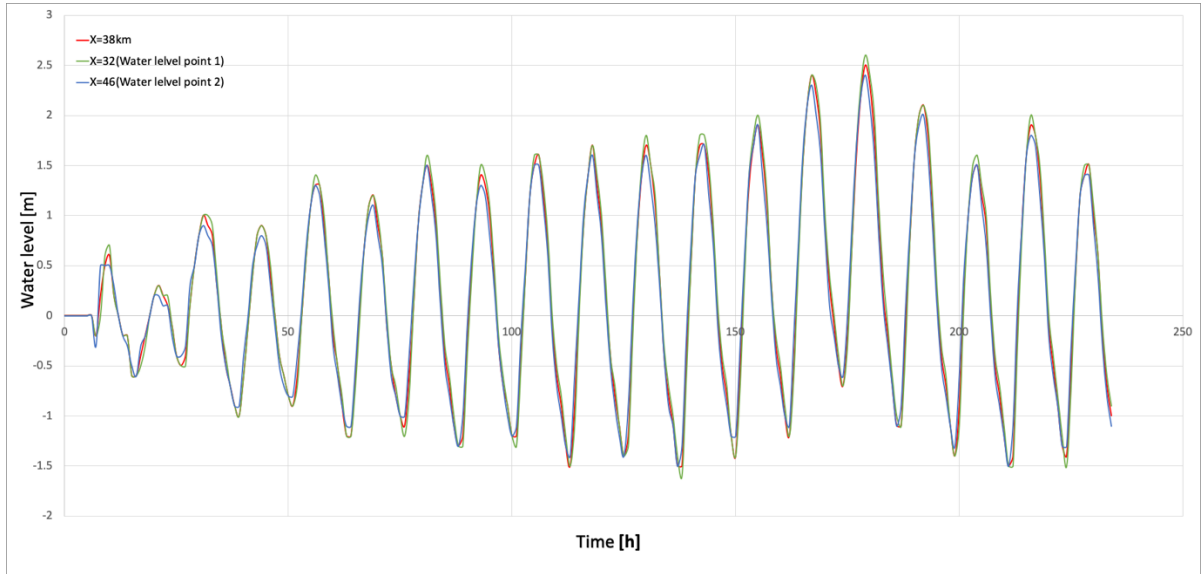


Figure 4.3: Water level variation of three locations (x=32,38,46)

By doing many similar analyses as stated above, the water level of other locations can be derived. The results are shown in Table 4.1

Table 4.1: Summary of water level condition

Distance along the sea dike alignment	Water level condition	Measured Station	Water level [WD]						
			Return period						
			1000	500	200	100	50	20	10
0km-38km	Water level 1	Wusongkou	6.6	6.44	6.21	6.04	5.87	5.63	5.44
38km-56km	Water level 2	Gaoqiao	6.94	6.73	6.43	6.21	5.98	5.68	5.44
56km-84km	Water level 3	Sanjiagang	6.82	6.6	6.3	6.07	5.83	5.52	5.27
84km-160km	Water level 4	Luchaogang	6.42	6.24	5.99	5.8	5.62	5.37	5.18
160km-210km	Water level 5	Jinshanzui	7.34	7.13	6.83	6.6	6.37	6.06	5.82

Combining other variables, the section division results are shown in Figure 4.4.

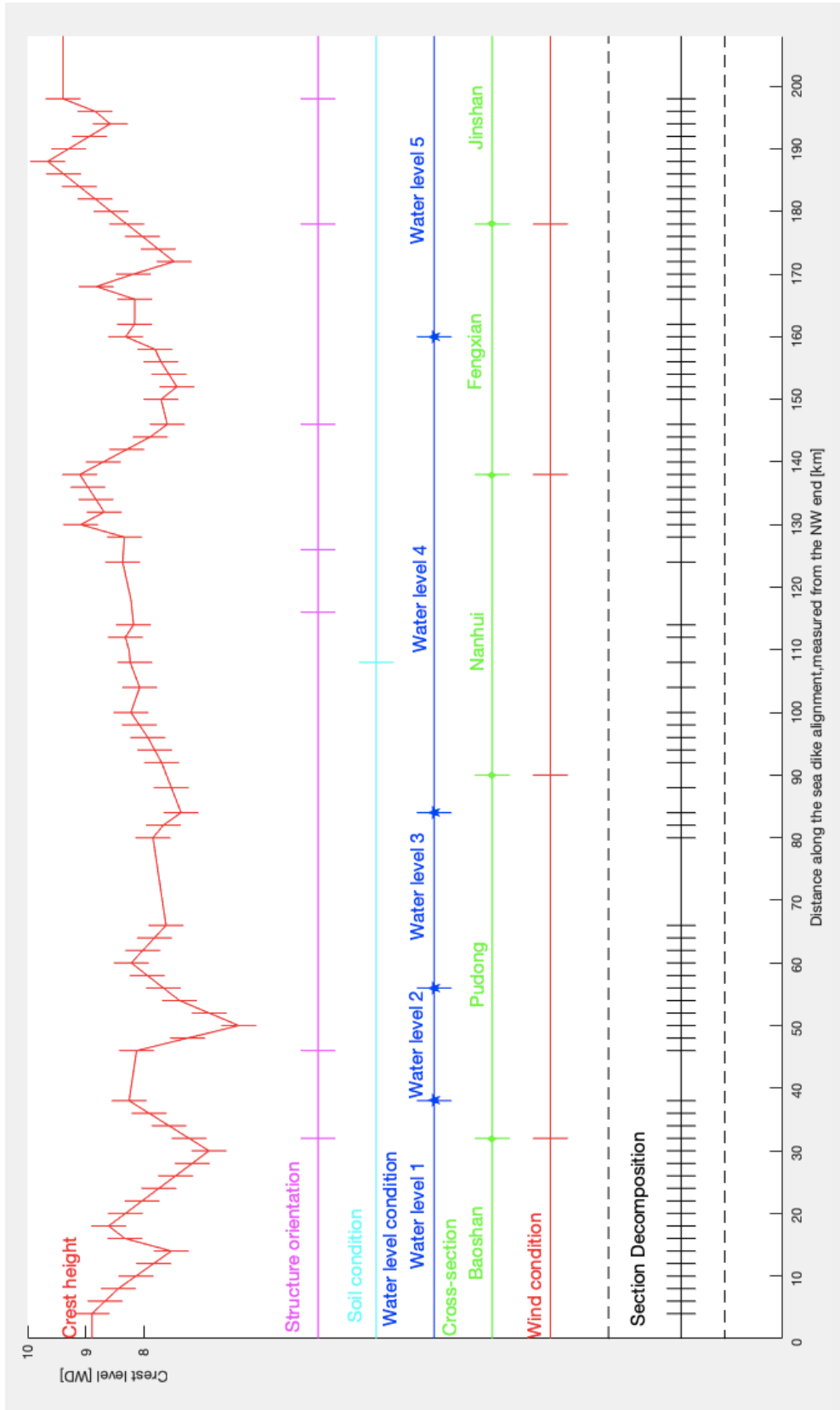


Figure 4.4: Section decomposition.

As a result, Figure 4.4 illustrates how decomposition was implemented:

1. The red curve represents the variation of the crest level along the coastline. According to its intensity of variation, 78 cut-off points were defined, complying with the above-mentioned principle.
2. According to the orientation of the floodwalls, six cut-off points were defined. The detailed description of orientations is stated in Section 3.2.2(3).
3. Based on the Soil condition type, a cut-off point was laid in the middle part of the stretch. The soil conditions are shown in Section 3.2.3(1)
4. According to the previous analysis of the water level condition, four cut-off points were defined. The water level conditions are listed in Table 4.1
5. As stated before, the Shanghai system can be divided into five sub-divisions based on the cross-section types and political district boundaries, so four cut-off points were laid.
6. As for the wind condition including the water depth and fetch, the same four cut-off points were defined based on the previous wind data, which is stated in Section 3.2.1(2).

In summary, the system is decomposed into 79 segments (Baohsan:15 sections, Pudong:19 sections, Nanhui:16 sections, Fengxian:18 sections, Jinshan:11 sections). Within each segment, boundary conditions were distinct and entailed schematizing.

4.2 Overtopping/Overflow

Overtopping/overflow is a common failure mode for coastal flood defences. In this chapter, the limit state function and the related parameters will be discussed.

4.2.1 Limit state function

The failure mechanism overflow essentially considers whether the crest height of the dike is high enough to hold back extreme water levels. The limit state function for overflow is the difference between the dike height (H) and the water level (W)(S. Jonkman & Schweckendiek, 2015b).

$$Z = H - W \quad (4.1)$$

in which

H = crest elevation + crown wall height(WD)

W = water level (WD)

In theory, wave overtopping can be described by a limit state function (Equation 4.2), in which the 'load' is the actual wave overtopping rate q ; the 'strength' is a critical rate q_c which is higher than the limit for inundation. The reliability function(Allsop et al., 2007) is expressed by:

$$Z = q_c - q \quad (4.2)$$

in which

q_c = critical wave overtopping discharge ($m^3/m/s$)

q = actual wave overtopping discharge ($m^3/m/s$)

Therefore, the failure of overtopping or overflow failure will occur if Z calculated from Equation 4.1 or 4.2 is less than zero.

- **Chinese standard of overtopping calculation**

The actual overtopping rate can be calculated based on followed by a (Chinese) empirical overtopping function (Equation 4.3) for sea-dikes with crown walls (Ministry of Water Resources, 2014). Some parameters are shown in Figure 4.5.

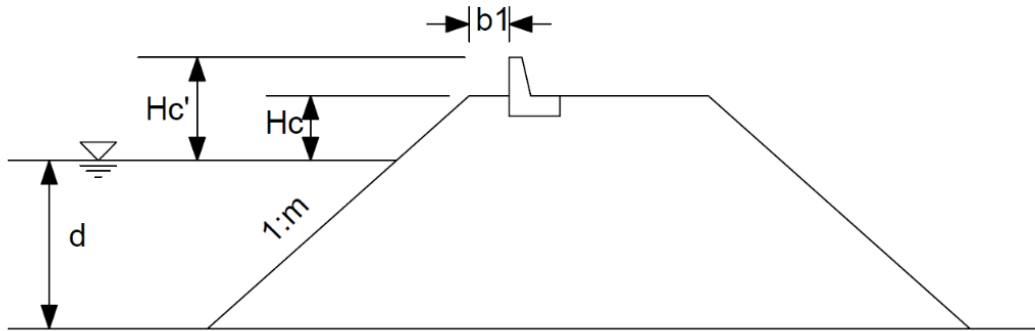


Figure 4.5: Sea embankment with seawall (Ministry of Water Resources, 2014)

$$q = 0.07 \frac{R_c}{H_s} \exp\left(0.5 - \frac{b_1}{2H_s}\right) B K_A \frac{H_s}{T_p} \left[\frac{0.3}{\sqrt{1/\tan\alpha}} + th\left(\frac{d}{H_s} - 2.8\right)^2 \right] \ln \sqrt{\frac{g T_p^2}{2\pi H_s \tan\alpha}} \quad (4.3)$$

in which

K_A = influence factor for roughness on the slope (-)

H_s = significant wave height at toe of the structure (m).

g = gravitational acceleration (m/s^2)

R_c = crest freeboard (m)

$\tan\alpha$ = outer slope angle (-)

d = water depth at toe of the structure (m)

T_p = peak period (s)

b_1 = distance of crown wall on the crest to the seaward (m)

B - empirical factor (-); this value is suggested as 0.6, 0.25, 0.38 when the value of $\tan\alpha$ is 1/1.5, 1/2, 1/3, respectively,

- **EurOtop calculation**

Based on EurOtop(Van der Meer et al., 2018), the formula (Equation. 4.4) is strongly recommended to be used for a design or assessment approach.

$$\frac{q}{\sqrt{gH_{m0}^3}} = \frac{f_a}{\sqrt{\tan\alpha}} \gamma_b \zeta_{m-1,0} \exp \left[- \left(f_b \frac{R_c}{\zeta_{m-1,0} H_{m0} \gamma_b \gamma_f \gamma_\beta \gamma_v} \right)^{1.3} \right] \quad (4.4)$$

in which

H_{m0} = significant wave height.

g = gravitational acceleration (m/s^2)

R_c = crest freeboard(m)

$\tan\alpha$ = outerslop angle(-)

$\zeta_{m-1,0}$ = Iribarren number which is defined as $\tan\alpha / (H_{m0}/L_{m-1,0})^{1/2}$ where α is the slope of the front face of the structure and $L_{m-1,0}$ being the deep water wavelength $gT^2_{m-1,0}/(2\pi)$.

γ_b = is the influence factor for a berm (-),

γ_f = is the influence factor for roughness elements on a slope (-),

γ_β = the influence factor for oblique wave attack (-)

γ_v = the influence factor for a wall at the end of a slope (-).

f_a, f_b =model factors, the mean value=0.023, 2.7, the standard deviation= 0.003,0.2.

Comparing the two formulae, the Chinese method is suitable for the dikes without berm, but the influence factors for a berm and oblique wave are included in the EurOtop formula. Since the Shanghai sea dikes are the composite structures, the influence of a berm needs to take into account. In this study, the EurOtop calculation (Equation 4.4) will be used to calculate the actual overtopping discharge.

In Equation 4.2, the critical discharge is introduced. It implies that the overtopping failure occurs if the discharge of inflow reaches a limit (i.e., q_c). According to the EurOtop(Van der Meer et al., 2018), the critical overtopping rate should follow the standard in Table 4.2 in design cases.

Table 4.2: Overview of calculation values for the critical overtopping discharge(en Milieu, 2016b)

q_c [l/m/s]	Additional requirements
0.1	<ul style="list-style-type: none"> • no requirements
1	<ul style="list-style-type: none"> • closed or open sod on clay * • no requirements for objects and transitions • sufficient stability **
5	<ul style="list-style-type: none"> • Applicable in two possible cases: <ul style="list-style-type: none"> - closed sod on clay * and $H_{m0} < 4$ m or - open sod on clay * and $H_{m0} < 2$ m • slope less than 1: 2.3 • no requirements for objects and transitions on the crown • no objects larger than 0.15 x 0.15 m² and no transitions on a slope • sufficient stability **

10	<ul style="list-style-type: none"> • closed sod on clay • slope less than 1: 2.3 • objects and transitions on the crown allowed (does not apply in the upper river area) • no objects larger than 0.15 x 0.15 m² and no transitions on a slope • H_{m0} <4 m • stability control **
<p>* Minimum guaranteed thickness of 0.4 m</p> <p>** Check whether the calculation value of the overtopping flow leads to an unacceptable increase in the failure probability as a result of the geotechnical instability of the covering on the inner slope or macro stability inwards. This can lead to additional requirements with regard to clay layer thickness, clay quality, application of drainage. slope and the like</p>	

The critical discharge is dependent on the backland area protected by the floodwall. Since the design standard of Shanghai sea dikes is ‘no overtopping’, considering the situation of the backland of Shanghai sea dikes (no maintained grass cover) and both Chinese and Dutch standards, the critical overtopping discharge q_c is assumed to be a deterministic value of 1 l/m/s in this study. To consider the sensitivity and the give reinforcement suggestions, 5 l/m/s and 10 l/m/s will also be discussed in the following part.

4.2.2 Parameters and Distributions

To calculate the failure probability of overtopping, parameters which are important in the limit state function and their characteristics of distribution are needed to be determined.

a. Hydraulic conditions

The essential hydraulic loads for overtopping/overflow are water level, significant wave height and spectral wave period. The water level condition and the characteristics of their distributions are stated in Section 3.2.1. Based on the fragility curve method stated in Section 2.2, the water levels are deterministic value in the calculation of failure probability.

As stated before, to derive the wind wave parameters, the fetch and water depth are important. According to the wave conditions (including wind speed, fetch, water depth...) and wind wave equations in Section 3.2.1, the significant wave height and the peak wave period can be derived. However, the spectral wave period instead of peak wave period is used in Equation 4.4, so the relationship between these two wave periods need to be taken into consideration.

Equation 4.5 gives the relation between peak period T_p and spectral period $T_{m-1,0}$ (Van der Meer et al., 2018).

$$T_p = 1.1T_{m-1,0} \quad (4.5)$$

However, the exact relation between T_p and $T_{m-1,0}$ is more complicated. According to Bas Hofland's research, an empirical prediction formula for $T_{m-1,0}$ is given in Equation 4.6(Hofland, Chen, Altomare, & Oosterlo, 2017).

$$\frac{T_{m-1,0,t}}{T_{m-1,0,o}} - 1 = 6 \exp(-4\tilde{h}) + \exp(-4\tilde{h}) \quad (4.6)$$

To know the exact relation between the T_p and $T_{m-1,0}$ for Shanghai sea dike condition, more flume tests and numerical calculations are needed. Due to lack of data, the factor 1.1 can be the first guess, and it can be assumed to be the normal distribution with mean value=1.1 and standard deviation=0.1.

b. Freeboard

The freeboard R_c is another important parameter for both overtopping and overflow which can be calculated by(Van der Meer et al., 2018):

$$R_c = H - W \quad (4.6)$$

In which

H = crest elevation + crown wall height;

W= water level, which can be assumed to be the extreme water level of different return periods.

The crest elevation and crown wall height data are summarized in Table 3.8. Crest elevation is a stochastic variable and it varies, dependent on the intensity of variation within each section. Therefore, the length of section and construction techniques can affect the crest level's uncertainty. The crown wall height can also be seen as a stochastic variable due to the quality and techniques of construction. These two variables are assumed to follow the Normal distribution, and the mean values are summarized in Table 3.8. The standard deviation of crest elevation was about 0.1m in the VNK2. The section length of the VNK2 is around 1km, in this study, most sections are around 2 km. Moreover, Shanghai also owns qualified construction quality the same as the Netherlands. Hence, it is reasonable to assume the standard deviation of crest elevation of 0.1m as that in the Netherlands. As for the crown wall height, due to its simple construction, the standard deviation can be assumed to be smaller than 0.1m, so 0.01 m was used to describe the smaller uncertainty.

c. Influence factor

- **Average slopes**

Many dikes consist of a composite profile with different slopes, a berm or multiple berms. A characteristic slope is required to be used in the breaker parameter $\xi_{m-1,0}$ for bermed

profiles to calculate wave overtopping. The average slope value can be calculated by (Van der Meer et al., 2018):

First estimate:

$$\tan\alpha = \frac{3H_{m0}}{L_{Slope} - B} \quad (4.7)$$

Second estimate:

$$\tan\alpha = \frac{(1.5H_{m0} + R_{u2\%}(\text{from 1st estimate}))}{L_{Slope} - B} \quad (4.8)$$

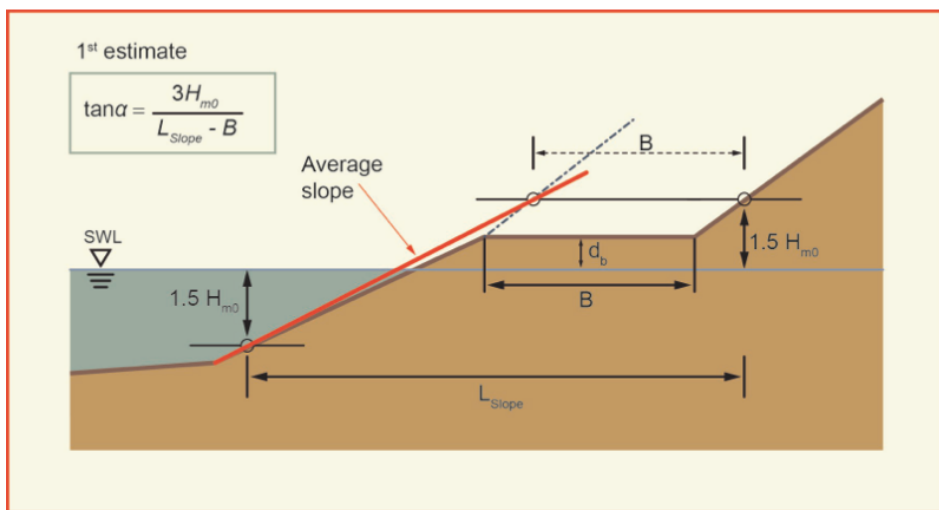


Figure 4.6: Determination of the average slope (1st estimate) (Van der Meer et al., 2018)

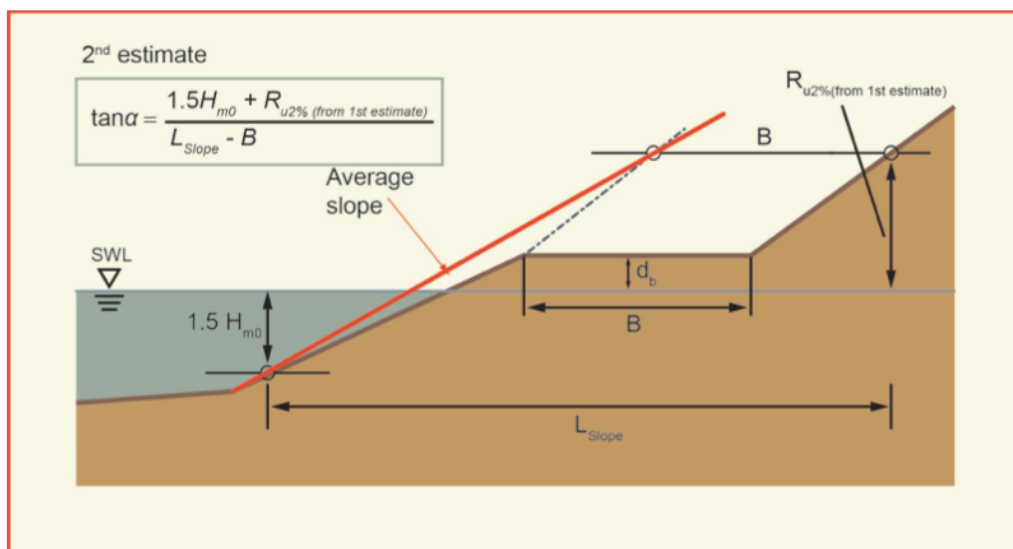


Figure 4.7: Determination of the average slope (2nd estimate) (Van der Meer et al., 2018)

- **Influence of berms**

A berm reduces wave overtopping. The influence factor γ_b for a berm consists of two parts, given by r_B and r_{db} . The influence factor γ_b can be calculated by (Van der Meer et al., 2018):

$$\gamma_b = 1 - r_B(1 - r_{db}) \quad \text{for: } 0.6 \leq \gamma_b \leq 1.0 \quad (4.9)$$

$$r_B = \frac{B}{L_{Berm}} \quad (4.10)$$

$$r_{db} = 0.5 - 0.5 \cos\left(\pi \frac{d_b}{R_{u2\%}}\right) \quad \text{for a berm above still water line} \quad (4.11)$$

$$r_{db} = 0.5 - 0.5 \cos\left(\pi \frac{d_b}{2H_{m0}}\right) \quad \text{for a berm below still water line} \quad (4.12)$$

$$r_{db} = 1 \quad \text{for berms lying outside the area of influence} \quad (4.13)$$

- **Influence of oblique waves**

For practical purposes, it is recommended to use the following expressions for short-crested waves to calculate the influence factor γ_β for wave overtopping (Van der Meer et al., 2018):

$$\gamma_\beta = 1 - 0.0033|\beta| \quad \text{for: } 0^\circ \leq \beta \leq 80^\circ \text{ (short - crested waves)} \quad (4.14)$$

$$\gamma_\beta = 0.736. \quad \text{for: } |\beta| \geq 80^\circ \quad (4.15)$$

- **Influence of roughness**

The influence factor γ_f is calculated by weighting the various influence factors $\gamma_{f,i}$ and by including the lengths L_i of the appropriate sections i in between $SWL-0.25 \cdot R_{u2\%smooth}$ and $SWL+0.50 \cdot R_{u2\%smooth}$ as follows (Van der Meer et al., 2018):

$$\gamma_f = \frac{\sum_{i=1}^n \gamma_{f,i} \cdot L_i}{\sum_{i=1}^n L_i} \quad (4.16)$$

The roughness factor γ_f depends on the types of the armour layer. As for Shanghai sea defences, there are two types of armour layers, Accropode and fence board. The influence factor of Accropode is 0.46 (Van der Meer et al., 2018).

As for the fence board which is a typical type of revetment which is widely used in China, the value of roughness of fence board is not clear in the Van der Meer formula, based on some researchers' studies in Appendix B, the roughness influence of fence board is shown in Equation 4.17

$$q_{fence\ board} = 0.8 \times q_{concrete} \quad (4.17)$$

According to this relation, the exact roughness factor of fence board for the EurOtop overtopping calculation can be derived by iterative approach:

1. Using Equation 4.3 and calculation the wave overtopping discharge q_1 with $\gamma_f=1$;
2. Considering the effect of fence board by multiplying q_1 with 0.8 to get the wave overtopping discharge q_2 ;
3. Iteratively determine the exact roughness factor γ_f for fence board for the q_2 .

Then the calculation the combined roughness factor by Equation 4.16, using the exact roughness factor γ_f for fence board and the roughness factor of Accropode can be implemented.

- **Influence factor for a wall at the end of a slope**

Measures at the crest level of a slope, such as vertical crown walls, can also reduce wave overtopping discharges.

The case of Shanghai sea dikes corresponds to the situation where a vertical wall (with height h_{wall}) is built on the top of the slope of the dike. The influence factor γ_v is defined as follows (Van der Meer et al., 2018):

$$\gamma_v = \exp\left(-0.56 \frac{h_{wall}}{R_c}\right) \quad (4.18)$$

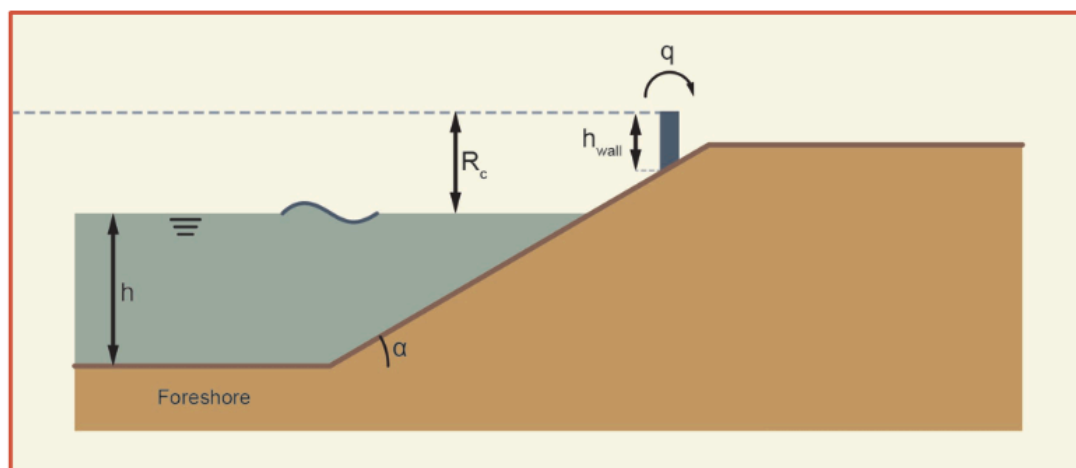


Figure 4.8: Configuration of a slope with a storm wall (Van der Meer et al., 2018)

4.3 Instability of armour unit

The instability of revetment layer can occur under the storm conditions induced by wave actions.

4.3.1 Revetment characteristics

There are many different revetment materials with different properties. For sea dikes in Shanghai, there are only two types of revetment materials:

a. Accropode

The Accropode is a single-layer artificial armour unit developed by Sogreah in 1981. Accropode concrete armour units are applied in a single layer(Bonfantini, 2014).



Figure 4.9: Accropode in Shanghai(Yin, 2020a)

b. Fence board

The concrete fence board is a kind of prefabricated component and has been applied in the anti-tidal embankment project in China since the 1980s, which has a great energy dissipation effect and good slope protection effect.



Figure 4.10: Fence board in Shanghai(Yin, 2020a)

The characteristics of the revetment layers of different sub-divisions are summarized in Table 4.3.

Table 4.3: Revetment characteristics

Sub-division	Revetment	
	Upper slope	Lower slope
Baoshan	Fence board(30cm)	Fence board(30cm)
Pudong	Fence board(30cm)	Fence board(30cm)
Nanhui	Accropode(3t)	Fence board(40cm)
Fengxian	Fence board(35cm)	Fence board(35cm)
Jinshan	Accropode(3t)	Fence board(30cm)

4.3.2 Limit State Function

a. Accropode

Damage when loose material starts to move. The load is the lift and drag forces acting on the stones of the cover layer by waves. The strength is the inertial forces and forces due to friction and interlocking(Morris, 2008).

The limit state equation is expressed as(Van, van Gelder, & Vrijling, 2007):

$$Z_{ac} = (K_D c o t \alpha)^{\frac{1}{3}} - \frac{H_s}{\Delta D_n} \quad (4.18)$$

in which

H_s = wave height at structure location (m)

D_n = Accropode unit diameter (m)

k_D = coefficient, 12-15 for permeable cores (Manual, 2007)

α = slope angle(°)

b. Fence board

Since there are only a few studies on the stability of fence board, the limit state function of the fence board can be expressed by the only the thickness actual(t_{actual}) and required(t_R) thickness of fence board(Ministry of Water Resources, 2014):

$$Z_{fb} = f_1 \frac{\gamma}{\gamma_c - \gamma} \frac{f_2 + f_3 \frac{d}{H}}{m^{0.27}} H - tr \quad (4.19)$$

in which

γ_c = unit weight of fence board (kN/m³). Here, $\gamma_c = 24$ (kN/m³)

γ = unit weight of water (kN/m³). Here, $\gamma = 10$ (kN/m³)

d = water depth (m)

H = wave height(m). When $d/L \geq 0.125$, $H = H5\%$. When $d/L < 0.125$, $H = H13\%$.

$m = \cot \alpha$ (outer slope).

f_1, f_2, f_3 =model factors.

4.3.3 Parameters and Distributions

The hydraulic conditions are stated in Section 4.2.2, other parameters that are important will be discussed in the following:

a. Coefficient k_D

In the limit state function of Accropode, a coefficient k_D was applied, the Rock manual gives a design value 12-15 for permeable cores(Manual, 2007). To do the probabilistic analysis, this coefficient can be assumed to be normal distribution with mean value=12 and standard deviation=0.6.

b. Revetment characteristics

Revetment characteristics like Accropode diameter and fence board thickness are summarized in Table 4.3, which are assumed to be deterministic since they are prefabricated.

The actual diameter D_n is the realistic diameter of Accropode, for this study three tons Accropodes are used and the equivalent cube size so the $D_n = 1.0\text{m}$ which can be found from Accropode design guide table.

c. Model factor

In the limit state function of fence board, three model factors f_1 , f_2 and f_3 were applied, the Code for design of sea dike project (Ministry of Water Resources, 2014) gives the design values of three factors which are 0.235, 0.61 and 0.13 respectively. To do the probabilistic analysis, these three factors can be assumed to be normal distribution with standard deviation=0.012, 0.0305 and 0.0065 respectively.

4.4 Macro instability

Macro-instability is defined as an unstable situation in which the ability of the dike to react to a disturbing force by maintaining or re-establishing its position has been compromised (CIRIA., 2013). When the active strengths of soil particles movement exceed the resistant strengths macro instability occurs (Groot, 2015).

4.4.1 Sliding of dike slopes (outer and inner slopes)

The basic macro-instability analysis consists of a driving moment, a resisting moment and the shear stress along the slip plane. The former moment is caused by the mass of soil at the water side of a circular slip plane, and the resisting moment is caused by the mass of soil at the land side (van Montfoort, 2018). For macro-stability the water level is an initiator, which will cause the increase of the pore water pressures. The weight of the soil does not change, but the change of resistance does will cause instability failure. In Figure 4.11 the basic principle of macro-instability is shown (S. Jonkman & Schweckendiek, 2015a).

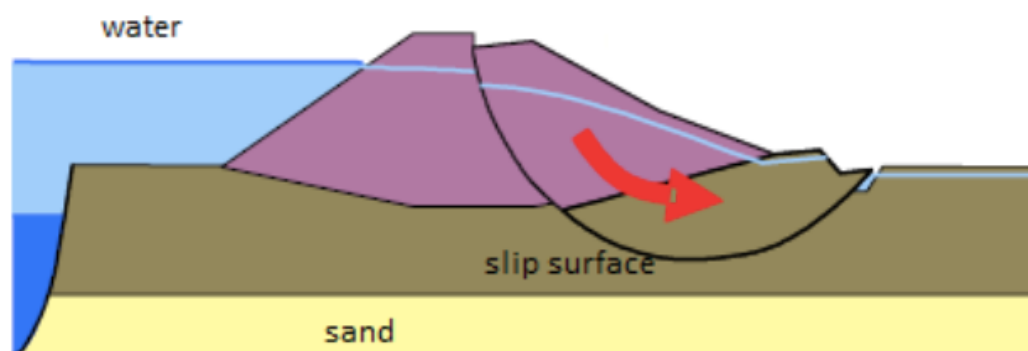


Figure 4.11: Basic principle of macro-instability (t Hart, De Bruijn, & De Vries, 2016)

4.4.2 Model and software

One of the most well-known slope stability assessment methods to determine the safety of a slope by means of limit equilibrium method 'LEM' is the one published by Bishop (1954)(Lin, Zhong, Xiong, & Tang, 2014). Limit equilibrium models (LEM) stems from the fact these models contemplate comparisons of the loads and resistances at the maximum mobilizable capacity for moment and force equilibria. When the loads exceed the resistance for either vertical/horizontal force or moment equilibrium, failure occurs.

The most widely used software for limit equilibrium slope stability analysis is D-Geo Stability(S. Jonkman & Schweckendiek, 2015b). D-Geo Stability is based on the *slip plane calculation methods* which finding out the most dangerous slip plane through numbers of calculations instead of directly indicating. Therefore, the slip plane with the lowest resistance to shearing ca be determined(Bischiniotis, 2013).

There are many different methods for slope stability in D-Geo Stability, and in this study the most commonly applied method Bishop was used. This methods takes into account the driving moments due to soil weight, water pressure and loads referenced to the center of a circular failure surface, as seen in Figure 4.12(Trompille & Eerninck, 2011).

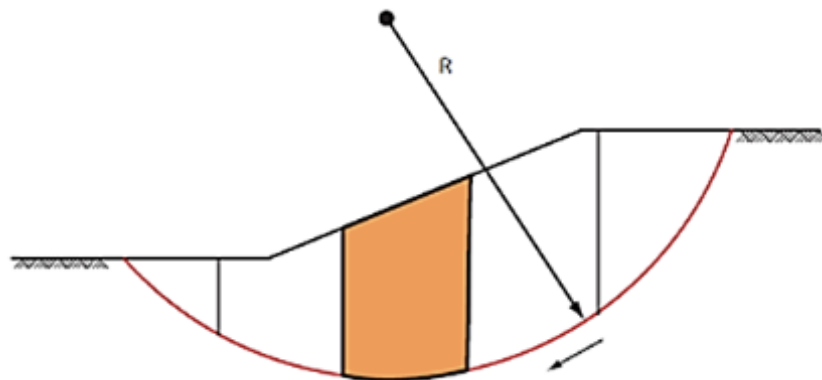


Figure 4.12: Assumed circular failure surface in the method of slices(Trompille & Eerninck, 2011)

4.4.3 Input data

a. Geometry

The typical geometry of the Shanghai sea dikes of different sections are shown in Figure 3.13.

b. Soil property

Soil properties was collected and is given in Figure 4.13, and the properties of each soil layer including parameters and their distributions are shown in Table 3.10 and Table 3.11.

According to these, it can be derived that a large proportion of the soil is silt and clay(thickness>20m). Clay and silt are compressible, relatively impermeable and have less shear strength.

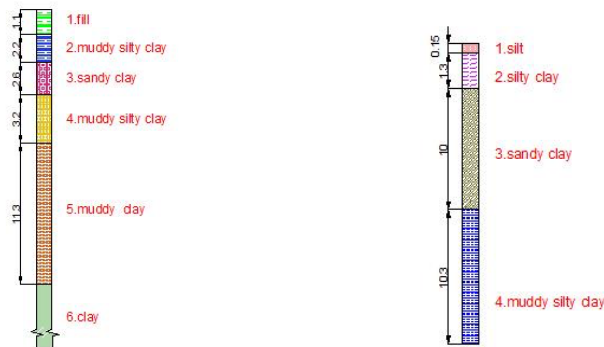


Figure 4.13: Soil layer distribution(Left: Soil layer of Baoshan and Pudong; Right: Soil layer of Nanhui, fengxian and Jinshan)

c. Phreatic line

The position of the phreatic surface mainly depends on the the water level and the permeability of the materials in the dike body, and the duration of the flood loading. Due to the lack of the phreatic surface data, numerical models can be used to analyze seepage of dike using FEM based software i.e. the SEEP/W. The numerical model SEEP/W can be employed to carry out simulation of seepage and phreatic surface.

An example result of the seepage analysis and phreatic line are shown in Figure 4.14, and other phreatic line of different sections under different water levels can also be modelled by Seep/W. The detailed modelling method is in Appendix C.

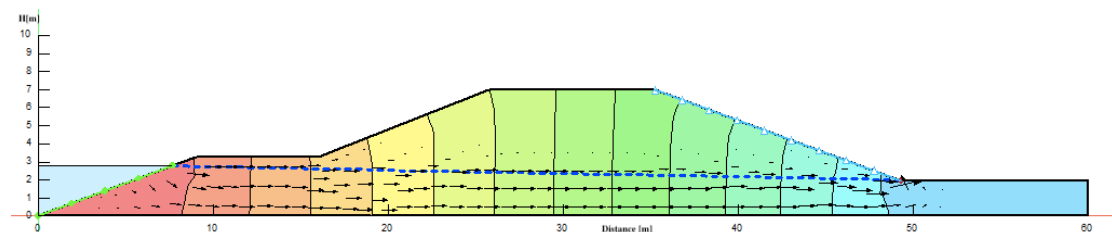


Figure 4.14: Example of phreatic line (Pudong, 10-year return period water level condition)

4.4.4 Model set up

Figure 4.15 shows the geometry of Section 1 as schematized in the D-GeoStability software as an example.

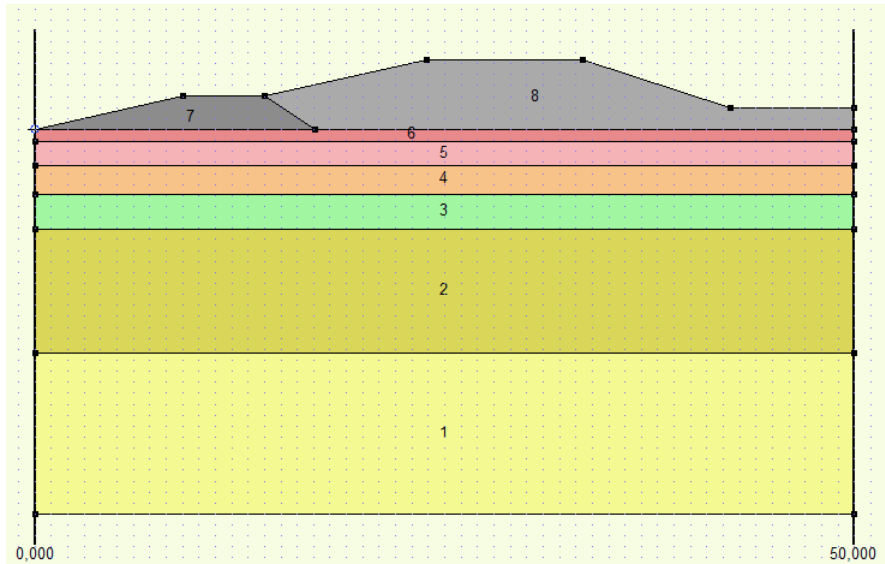


Figure 4.15: Dike geometry of Section 1 as schematized in D-GeoStability

After setting all the features, a D-Geo Stability file is created and D-Geo Stability performs the probabilistic simulation, the probability of failure for this water level. The probability of failure can be derived from the software D-Geo Stability.

4.5 Variables summary

In summary, the dike could fail mainly due to overtopping/overflow, revetment instability, Macro-instability. Limit state functions are stated in previous sections and distributions of involved variables were assigned. Table 4.4 is a list of all the relevant variables and their distributions.

Table 4.4: : List of variables

Variable	Parameter	Unit	Distribution	Mean	Standard deviation	Variation coefficient
Wind speed	U	m/s	P-III	Table 2.7		
Crest elevation	h_crest	WD	normal	Figure 2.6	0.1	-
Crown wall height	h_wall	m	Normal	1.2	0.01	0.0083
Fetch	F	m	Normal	Table 2.8	-	0.07

Water depth	d	m	Normal	Table 2.8	0.2	-
orientation	or	°	Deterministic	Table 2.10	-	-
Water level	WL	WD	Deterministic	Table 2.1	-	-
Slope angle	m	-	Deterministic	1/3	-	-
Bottom elevation	h_bottom	WD	Normal	Table 2.9	0.1	-
Berm elevation	h_berm	WD	Deterministic	Table 4.5	-	-
Berm width	B	m	Deterministic	Table 4.5	-	-
Model factor 1	f_a	-	Normal	0.023	0.003	0.13
Model factor 2	f_b	-	Normal	2.7	0.2	0.074
Model factor 3	f_c	-	Normal	1.1	0.1	0.09
Density of water	p_w	kg/m ³	Normal	1030	5	0.005
Density of concrete	p_s	kg/m ³	Normal	2400	10	0.004
Coefficient K _D for Accropode	KD	-	Normal	12	0.6	0.05
Accropode unit diameter	Dn	m	Deterministic	1.0	-	-
slope	cotalpha	-	Normal	3	0.15	0.05
Model factor 4	f1	-	Normal	0.235	0.012	0.05
Model factor 5	f2	-	Normal	0.61	0.0305	0.05
Model factor 6	f3	-	Normal	0.13	0.0065	0.05
Fence board thickness	tr	m	Deterministic	Table 4.3	-	-
Soil weight	gamma	kg/m ³	Normal	Table 2.11 and 2.12		
Cohesion	C	kPa	Normal			
Friction angle	Phi	°	Normal			

4.6 Customized model

A Matlab model is built on the probabilistic toolbox in OpenEarth which provides First Order Reliability Method (FORM) and Monte Carlo Simulation (MCS). In this study, MCS was selected to use in this study because it can provide relatively accurate results once the number of samples was sufficiently large.

4.7 Model Results

The output of the Matlab and Geostability models give the conditional failure probability per section. Table 4.5 gives the conditional failure probability of overtopping as an example. In this table, the water level with return periods of 1,000 years is adopted for example.

Table 4.5: Conditional failure probability of the overtopping under 1000-year water level condition

District	Section number	wind direction			
		N	NE	E	SE
baoshan	1	0.343	0.0274	0.0363	—
	2	0.3573	0.0295	0.0433	—
	3	0.3974	0.0439	0.0591	—
	4	0.4638	0.0668	0.0778	—
	5	0.5364	0.0909	0.1113	—
	6	0.6126	0.1307	0.1544	—
	7	0.5438	0.0979	0.1252	—
	8	0.4298	0.0481	0.0642	—
	9	0.4298	0.0481	0.0642	—
	10	0.4875	0.07	0.0872	—
	11	0.5622	0.0992	0.128	—
	12	0.6464	0.1407	0.1689	—
	13	0.745	0.1964	0.2324	—
	14	0.8577	0.2544	0.3157	—
	15	0.8429	0.2489	0.2933	—
pudong	16	0.2636	0.0641	0.0744	—
	17	0.2095	0.0514	0.0529	—
	18	0.1738	0.0371	0.0433	—
	19	0.2551	0.0375	0.043	—
	20	0.3239	0.0448	0.049	—
	21	0.5638	0.0891	0.104	—
	22	0.6471	0.0967	0.121	—
	23	0.4557	0.0671	0.0736	—
	24	0.3527	0.0506	0.0554	—
	25	0.3204	0.0344	0.0355	—
	26	0.2757	0.0298	0.0372	—
	27	0.2752	0.0252	0.0311	—
	28	0.3016	0.0324	0.0358	—
	29	0.3358	0.0372	0.0426	—
	30	0.3218	0.0355	0.042	—
	31	0.3255	0.0381	0.0421	—
	32	0.3702	0.0462	0.0523	—
	33	0.2061	0.045	0.0498	—
	34	0.1958	0.0367	0.0444	—
	35	0.9609	0.5341	0.6066	0.9990
	36	0.9383	0.4876	0.5605	0.9966

north part of Nanhui	37	0.9283	0.4602	0.5314	0.9929
	38	0.9096	0.4118	0.5014	0.9893
	39	0.8875	0.3545	0.4661	0.9820
	40	0.8875	0.3545	0.4661	0.9820
	41	0.8875	0.3545	0.4661	0.9820
District	Section number	wind direction			
		S	SW	E	SE
south part of Nanhui	42	0.8393	0.087	0.1517	0.2005
	43	0.8435	0.0874	0.1499	0.1973
	44	0.8464	0.0904	0.1514	0.2004
	45	0.8257	0.0749	0.1341	0.1897
	46	0.7394	0.0332	0.0844	0.1489
	47	0.7087	0.0193	0.0637	0.1326
	48	0.7265	0.0301	0.0799	0.1417
	49	0.7116	0.0219	0.0583	0.13
	50	0.6773	0.0146	0.0466	0.1129
Fengxian	51	0.2587	0.0306	0.0331	0.0401
	52	0.3297	0.0423	0.0429	0.0589
	53	0.4028	0.0557	0.0667	0.1102
	54	0.5005	0.0738	0.0885	0.1088
	55	0.521	0.0858	0.0943	0.1222
	56	0.5415	0.0898	0.1042	0.1261
	57	0.5621	0.0957	0.1135	0.1377
	58	0.5304	0.088	0.0983	0.1213
	59	0.4904	0.0782	0.0866	0.1163
	60	0.4122	0.056	0.068	0.0829
	61	0.8875	0.1048	0.1558	0.2562
	62	0.9018	0.1118	0.1667	0.2744
	63	0.8264	0.0884	0.1307	0.2241
	64	0.8193	0.0866	0.138	0.2208
	65	0.9693	0.1358	0.2113	0.3212
	66	0.9915	0.1602	0.239	0.3492
	67	0.9589	0.1337	0.1968	0.2995
	68	0.9059	0.1118	0.1667	0.2744
Jinshan	69	0.8393	0.087	0.1517	0.2005
	70	0.8435	0.0874	0.1499	0.1973
	71	0.8464	0.0904	0.1514	0.2004
	72	0.8257	0.0749	0.1341	0.1897
	73	0.7394	0.0332	0.0844	0.1489
	74	0.7087	0.0193	0.0637	0.1326
	75	0.7265	0.0301	0.0799	0.1417

	76	0.7116	0.0219	0.0583	0.13
	77	0.6773	0.0146	0.0466	0.1129
	78	0.2587	0.0306	0.0331	0.0401
	79	0.3297	0.0423	0.0429	0.0589

Chapter 5 System Reliability Analysis

In this chapter, the reliability of each section and each failure mechanism is combined into the reliability of the entire system. Moreover, the safety standard and required level of reliability are also implemented to assess the safety of Shanghai sea dikes.

5.1 Fault Tree

In the VNK2 project, failure mechanisms were schematized in fault trees. For a dike section, the failure may occur since there will present any failure mechanism. After being combined with the actual situation in Shanghai, they are modified and presented in Figure 5.1.

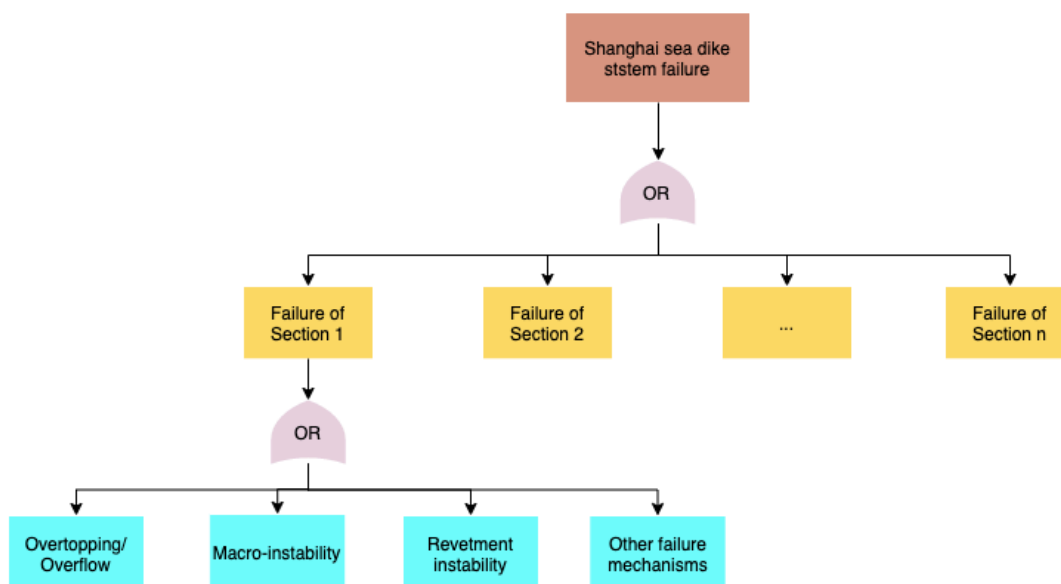


Figure 5.1: Fault tree of Shanghai sea dike system.

5.2 Contributions of Wind Direction

5.2.1 Direction-induced Conditional Failure Probability

Figure 5.2 indicates how wind direction contributes to the results. The overtopping failure probability of one specific section is calculated for each wind direction respectively, and then combining the failure probability to derive the final failure probability for the section by Equation 5.1.

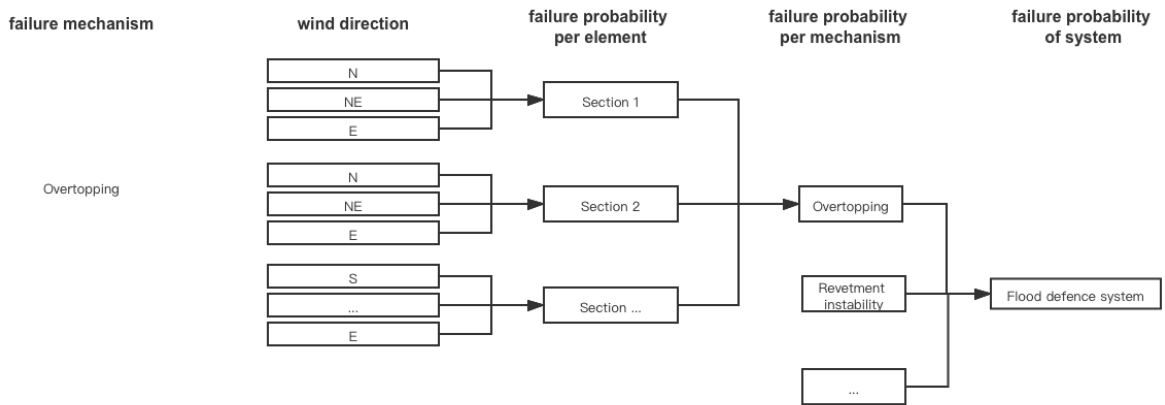


Figure 5.2: Flow chart for the failure of a flood defence system

$$P_f = \sum_{i=1}^n P(f|\varphi_i) P(\varphi_i). \quad (5.1)$$

in which:

$P(\varphi_i)$ = probability of occurrence of wind direction φ_i (e.g., N, NE)

P_f = failure probability of one failure mode for one segment

$P(f|\varphi_i)$ = failure probability given wind condition φ_i

5.2.2 Wind Direction in Shanghai

According to the Shanghai Engineering Construction Code, the occurrence probabilities of wind direction of Baoshan, Pudong, Nanhui, Fengxian and Jinshan five sub-divisions are summarized in Table 5.1.

Table 5.1: Summary of the occurrence probability of main wind direction(Shanghai Institute of Building Research Company 2011)

Sub-divison	Main wind direction	Occurrence probability (%)
Baoshan	N	4.6
	NE	10.3
	E	7.4
Pudong	N	1.6
	NE	6.0
	E	13.7
Nanhui	N	9.6
	NE	6.8
	E	6.3
	SE	8.0
	S	8.7
	SW	1.7

Fengxian	S	4.2
	SW	1.5
	E	7.6
	SE	9.5
Jinshan	S	3.8
	SW	2.3
	E	11.6
	SE	7.8

After considering the occurrence probability of wind directions, the failure probability result of three main failure mechanism under 1000-year water level condition is listed in Table 5.2.

Based on the results, overtopping is the most influential failure mode, and its conditional probability is at least 100 times higher than macro-instability and revetment failure. The section 35 (shown in Figure 5.3) gives the largest overtopping failure probability (around 0.302).

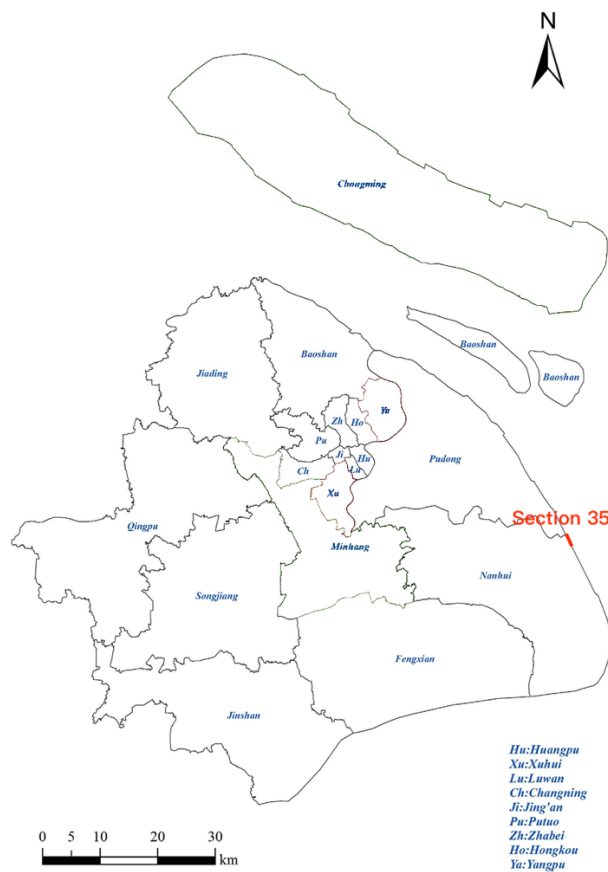


Figure 5.3 Location of Section 35

Macro-instability is the second most important failure modes. However, the failure probability is 100 times less than the overtopping.

Revetment failure is the least important failure mechanism among the three, and it is only significant in section 35-41 and section 69-79 under 1000-year water level condition. Revetment failure in other sections under 1000-year water level condition and all sections under 10, 50, ... 500 -water level condition is negligible.

“NaN” means that the frequency of occurrence in the 1,000,000 Monte Carlo samples was 0, but the failure probability was not necessarily 0. To be precise, the failure probability was supposed to be smaller than 1/1,000,000.³

Table 5.2: Conditional failure probability of the sub-division under 1000-year water level condition

Section number	Overtopping	Revetment	Macro-stability
1	8.54E-02	NaN	3.65E-04
2	9.00E-02	NaN	4.54E-04
3	1.01E-01	NaN	4.37E-04
4	1.15E-01	NaN	1.90E-04
5	1.35E-01	NaN	7.67E-05
6	1.53E-01	NaN	1.39E-04
7	1.37E-01	NaN	1.95E-04
8	1.06E-01	NaN	1.53E-04
9	1.06E-01	NaN	1.53E-04
10	1.22E-01	NaN	2.52E-04
11	1.40E-01	NaN	9.02E-05
12	1.59E-01	NaN	1.34E-04
13	1.78E-01	NaN	6.58E-05
14	2.00E-01	NaN	9.09E-05
15	1.98E-01	NaN	9.09E-05
16	5.13E-02	NaN	6.15E-06
17	4.28E-02	NaN	4.34E-06
18	3.52E-02	NaN	1.14E-05
19	5.57E-02	NaN	1.47E-05
20	6.56E-02	NaN	4.06E-06
21	1.05E-01	NaN	3.59E-06
22	1.19E-01	NaN	7.73E-07
23	8.65E-02	NaN	2.44E-06
24	6.94E-02	NaN	5.23E-06

³ Based on the following analysis, the combined probability of revetment failure is determined by the maximum section failure probability(magnitude: 1E-04), so the “NaN” represents a failure probability smaller than 1E-06 will not affect the combined system failure probability. Hereafter, the “NaN” can be regarded as the value of 0.

25	5.27E-02	NaN	3.90E-06
26	4.60E-02	NaN	8.25E-06
27	4.53E-02	NaN	9.54E-06
28	4.97E-02	NaN	3.22E-06
29	5.56E-02	NaN	4.02E-06
30	5.39E-02	NaN	4.02E-06
31	5.42E-02	NaN	4.02E-06
32	6.09E-02	NaN	4.44E-06
33	3.20E-02	NaN	3.08E-06
34	2.91E-02	NaN	3.06E-06
35	3.02E-01	1.59E-05	1.23E-08
36	2.98E-01	1.59E-05	1.42E-08
37	2.96E-01	1.59E-05	1.42E-08
38	2.92E-01	1.59E-05	4.33E-05
39	2.87E-01	1.59E-05	1.01E-04
40	2.87E-01	1.59E-05	1.01E-04
41	2.87E-01	1.59E-05	1.01E-04
42	2.15E-01	NaN	1.14E-04
43	2.15E-01	NaN	1.14E-04
44	2.15E-01	NaN	1.14E-04
45	2.12E-01	NaN	1.10E-04
46	1.94E-01	NaN	2.29E-04
47	1.87E-01	NaN	2.58E-04
48	1.93E-01	NaN	2.55E-04
49	1.88E-01	NaN	2.45E-04
50	1.80E-01	NaN	1.85E-04
51	1.25E-01	NaN	1.04E-06
52	1.46E-01	NaN	4.98E-07
53	1.67E-01	NaN	2.77E-07
54	1.86E-01	NaN	1.26E-07
55	1.90E-01	NaN	1.11E-07
56	1.93E-01	NaN	1.21E-07
57	1.96E-01	NaN	7.85E-08
58	1.91E-01	NaN	1.11E-07
59	1.85E-01	NaN	1.56E-07
60	1.69E-01	NaN	2.79E-07
61	2.18E-01	NaN	6.84E-07
62	2.19E-01	NaN	7.57E-07
63	2.15E-01	NaN	1.06E-06
64	2.15E-01	NaN	1.06E-06
65	2.24E-01	NaN	4.12E-07

66	2.26E-01	NaN	2.64E-07
67	2.23E-01	NaN	4.64E-07
68	2.19E-01	NaN	6.83E-07
69	2.13E-01	9.57E-04	1.08E-04
70	2.02E-01	9.57E-04	1.24E-04
71	1.92E-01	9.57E-04	2.18E-04
72	1.81E-01	9.57E-04	2.15E-04
73	1.69E-01	9.57E-04	4.11E-04
74	1.72E-01	9.57E-04	4.22E-04
75	1.87E-01	9.57E-04	2.29E-04
76	2.00E-01	9.57E-04	1.26E-04
77	2.03E-01	9.57E-04	1.24E-04
78	1.87E-01	9.57E-04	2.29E-04
79	1.75E-01	9.57E-04	3.63E-04

5.2.3 Fragility Curve

The fragility curves indicate the conditional probability of various failure mechanisms. Figure 5.4 presents the fragility curves and the exceedance probability of Section 77 for example.

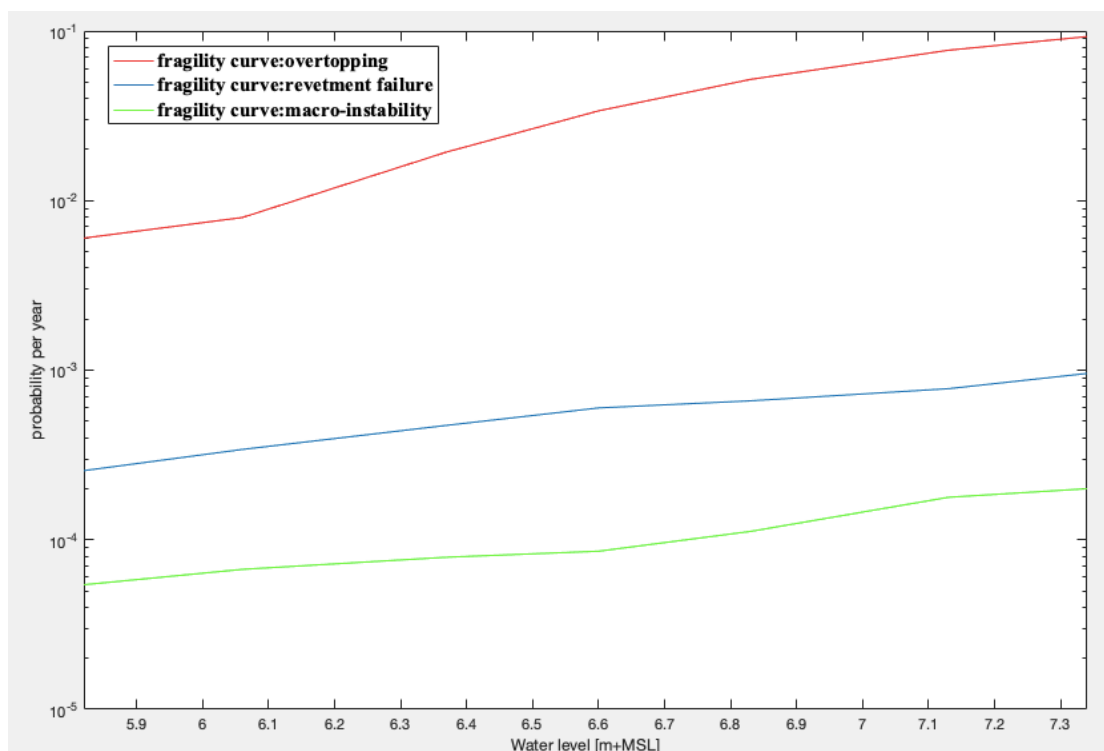


Figure 5.4 : Example of conditional failure probability (fragility curves) with the respect of water level (Section 77)

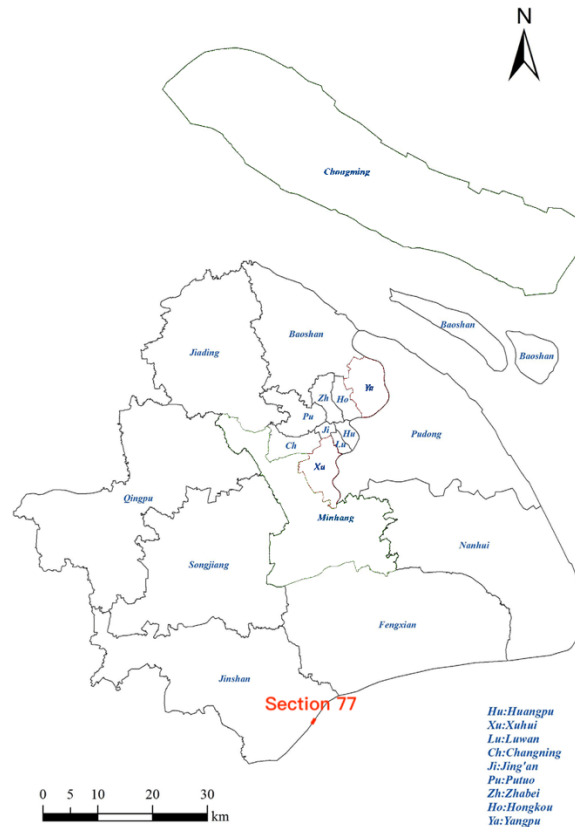


Figure 5.5 Location of Section 77

5.2.4 Failure Probability of the Sub-division

The second step is to use the numerical integration method provided that the probability distribution of the extreme water level is known. After the numerical integration, the unconditional failure probability of each mechanism and each section can be derived. The next step is to combine the unconditional failure probability.

In general, the components (i.e., segments plus failure modes) constitute a serial system in which the system would fail once one or more components failed (Z. Wang, 2016). The failure probability of sections can be combined to the system. The combination results would be affected by the correlations between dike sections. Some methods could be applied for estimation about correlation such as Hohenbichler method and Ditlevsen method. Due to the lack of information of dependency between dike sections, the correlation is not dealt with in this part. Instead, the elementary lower and upper bounds were simply taken.

There are usually two steps to combine the failure probability: 1) to combine the failure probability with the respect of failure mechanisms; 2) to combine the failure probability with the respect of flood defence sections (Z. Wang, 2016).

In this study, since the correlation is not taken into consideration, the former step is taken first and the failure probability per failure mechanism can be derived. The steps are visualized in Figure 5.6.

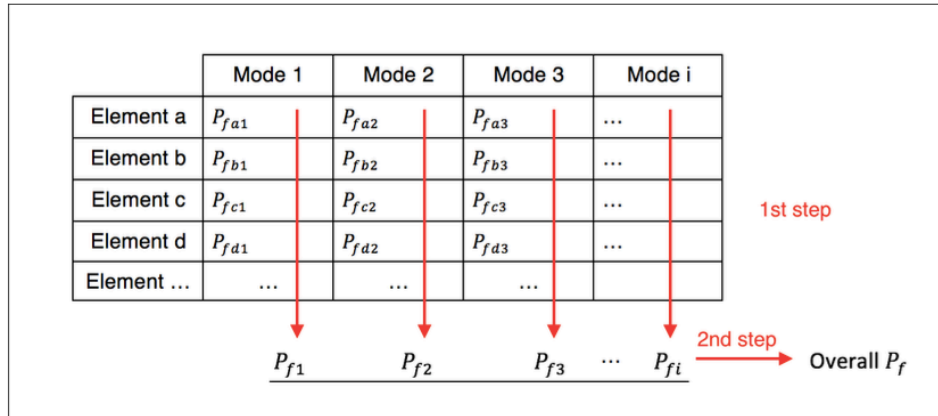


Figure 5.6: Process of combination(Z. Wang, 2016)

A group of dike sections is modelled as a series system and the elementary lower, upper bounds were simply taken shown in Table 5.3. For complete independent or fully dependent sections, the probability of failure can be calculated analytically. Based on the methods, the upper, lower boundaries can be derived for each sub-division of Shanghai sea dikes, shown in Table 5.4. These boundaries are too wide, the Ditlevsen boundaries are much narrower. However, a large number of calculations need to be done to get the Ditlevsen boundaries for the Shanghai sea dikes system. Although the linear programming analysis can help with the calculation, it still needs to consider 2^{79} variables which will be too time consuming (Song & Der Kiureghian, 2003). Moreover, the correlations between sections also need to consider, which requires extra analysis and dataset. Therefore, this will not be included in this study.

Table 5.3: Elementary bounds for probability of a series system failure

	Mutually exclusive sections	Independent sections	Fully dependent sections
	Upper boundary	Independent	Lower boundary
Series system	$P_{f,system} = \sum_{i=1}^n P_{f,i}$	$P_{f,system} = 1 - \prod_{i=1}^n P_{f,i}$	$P_{f,system} = MAX(P_{f,i})$

Table 5.4: Elementary bounds of each sub-division of Shanghai sea dikes

Sub-division		overtopping	Revetment failure	Macro-instability
Baoshan	upper bound	8.80E-02	0	5.03E-04
	lower bound	1.30E-02	0	8.33E-05
	Independent	8.45E-02	0	5.03E-04
Pudong	upper bound	3.63E-02	0	2.35E-05

	lower bound	4.24E-03	0	8.44E-06
	Independent	3.57E-02	0	2.35E-05
Nanhui	upper bound	2.69E-01	1.27E-07	2.67E-04
	lower bound	3.31E-02	1.59E-08	4.69E-05
	Independent	2.38E-01	1.27E-07	2.67E-04
Fengxian	upper bound	2.79E-01	0	1.38E-06
	lower bound	2.54E-02	0	1.86E-07
	Independent	2.46E-01	0	1.38E-06
Jinshan	upper bound	9.67E-02	1.73E-03	8.89E-04
	lower bound	1.24E-02	1.57E-04	4.73E-04
	Independent	9.26E-02	1.73E-03	8.89E-04

Overtopping/overflow is usually considered to be highly spatially correlated. Water levels and crest levels are usually the predominant factors that affect the reliability of segments against overtopping/overflow. They are usually correlated to a large extent. Therefore, for a simple approximation, a lower bound of $\max(P_i)$ was taken. However, in reality, the dependency among segments concerning overtopping and overflow might not be that high, so failure probability of it should be slightly higher than the lower bound.

As for the revetment stability, the wind direction effect will also be taken into consideration same as above. As for the combination of failure probability per section, the first step is similar to the method used in the overtopping part. The correlation with the respect of revetment failure highly depends on the types of the revetments and their sizes. For instance, the revetment in Baoshan part is fence board, so the correlation among the sections should be very high in this sub-division. Moreover, the wave height was another main factor that affect the failure probability when considering the failure probability of one sub-division. The wave heights could also be highly correlated in one sub- division, so the lower bound of $\max(P_i)$ was applied.

In terms of macro-instability, length effects make great contributions. The correlation with the respect of macro-stability failure highly depends on the cross-section profile and the soil type. For instance, from Section 1 to Section 15, the soil type and cross-section profile are homogeneous, so the correlation among them should be very high. In contrast, the correlation between Section 1 and Section 35 is very low, because they have completely different soil types. However, assumptions were made that only two types of soil conditions were adopted along the Shanghai sea dikes due to the lack of data. In reality, the number of types of soil types must be more than two. Conservatively, the upper bound of $P_i = \sum P_i$ was applied for this failure mode. Based on this, the failure probability of sections can be combined into the failure probability of each sub-division shown in Table 5.5.

Table 5.5: Unconditional failure probability of each sub-division

Sub-division	overtopping	Revetment failure	Macro-instability
Baoshan	1.30E-02	0	5.03E-04
Pudong	4.24E-03	0	2.35E-05
Nanhui	3.31E-02	1.27E-07	2.67E-04
Fengxian	2.54E-02	0	1.38E-06
Jinshan	1.24E-02	1.73E-03	8.89E-04

According to the result, Nanhui part has the largest failure probability of overtopping/overflow mechanism and Jinshan part has the largest failure probability of revetment and macro-instability. The failure probability of Baoshan is smaller compared to other four sub- divisions. The reason of this may be that the Baoshan part is sheltered by Chongming island, so the effect of the wind wave may be smaller. As for the revetment failure, except Nanhui and Jinshan, the failure probability of other three sub- divisions are negligible.

5.2.5 Combination of Failure Modes

As stated above, the Shanghai sea dike can be assumed to be a series system, since the correlations between different failure mechanisms are unknown. For complete independent failure mechanisms, the combined probability is the summation of the individual probabilities, for dependent failure mechanism the combined probability is equal to the highest probability of the individual scenarios.

$$\text{Max}(P_{f,i}) \leq P_{f,system} \leq 1 - \prod_{i=1-n}^n (1 - P_{f,i}) \quad (5.2)$$

Based on the Equation 5.2, the total failure probability of the Shanghai sea dike system can be derived, which is 3.31E-02 — 3.64E-02, shown in Table 5.6.

Table 5.6: Combined failure probability

Sub-division	overtopping	Revetment failure	Macro-instability	Total
Baoshan	1.30E-02	0	5.03E-04	-
Pudong	4.24E-03	0	2.35E-05	-
Nanhui	3.31E-02	1.27E-07	2.67E-04	-
Fengxian	2.54E-02	0	1.38E-06	-
Jinshan	1.24E-02	1.73E-03	8.89E-04	-
Combined	3.31E-02	1.73E-03	1.68E-03	3.31E-02 — 3.64E-02

5.3 Sensitivity Analysis

Based the previous results, the overtopping can be seen as the most important failure mechanism to see how critical overtopping discharge and crest height will influence the failure probability, which can also help give recommendations for the further reinforcement.

The calculation process is the same, so the detailed of process will not be introduced. The calculation failure probabilities by changing the critical overtopping discharge from 1 l/m/s to 5 l/m/s and 10 l/m/s, increasing the crest elevation of all sections with 0.5m and 1m

Table 5.7 Sensitivity analysis results

qc [l/m/s]	1	5	10
Overtopping failure probability [-]	3.31E-2	5.77E-3	1.68E-3
Total failure probability [-]	3.31E-02 — 3.64E-02	5.77E-03 — 9.18E-03	1.68E-03 — 5.09E-03
Crest elevation[WD]	Current	Current+0.5[m]	Current+1[m]
Overtopping failure probability [-]	3.31E-2	3.05E-3	1.94E-3
Total failure probability [-]	3.31E-02 — 3.64E-02	3.05E-03 — 6.46E-03	1.94E-03 — 5.35E-03

5.4 Safety Assessment

5.4.1 Safety standard

To assess whether the sea dike is safe or not, the safety standard needs to be derived first. In the year 2014 the Dutch government, as part of the delta program, introduced new safety standards for flood defences. The new standards became formal on January 1st, 2017, which is shown in Figure 5.7 The new safety standards were decided based on an advanced risk assessment of individual, societal and economic risk using cost-benefit analysis(Slomp, Knoeff, Bizzarri, Bottema, & de Vries, 2016).



Figure 5.7: Risk-based safety standards for flood defences(Slomp et al., 2016)

However, there is no clear safety standard that can be used for safety assessment for Shanghai sea dike. The design safety level of Shanghai sea dikes is 1/100-1/200, but this standard is not real safety standard. To derive the real safety standard, the cost benefit analysis needs to be done which will not be in this study since the cost-benefit analysis is out of the scope of this study. A simplified comparison of individual, societal and economic risk between flood defence in the Netherlands (Levee system 14: Zuid-Holland shown in Figure 5.8) and Shanghai sea dike will give an insight of the safety standard.



Figure 5.8: Location of Zuid Holland. (Vergouwe, 2016)

a. Economic Risk

The economic risk is the annual expected value of economic losses, expressed in euros per year, and it depends heavily on the economic value of an area. The protected area of Levee system 14 is very important to the Dutch economy, as 65% of the country's GNP is generated there. (Vergouwe, 2016) With a probability of flooding of the dike ring of 1/2500 per year, the economic risk for dike ring area 14 amounts to 2.3 million euros per year. The greatest damage amounts to 37 billion euros and takes place during a three-fold breach at Katwijk, Scheveningen Boulevard and Ter Heijde. (en Waterstaat & Waterbouwkunde, 2005)

As for Shanghai, Ke did the analysis of the Shanghai economic flood risk and gave an estimated value of 2-6 million USD/year (1.7-5.2 million euros/year) based on 26 flood scenarios (for the river flood risk instead of coastal flood risk), which will be seen as the preliminary results since the lack of coastal flood risk of Shanghai area.

b. Individual risk

The individual risk indicates the probability of death for a person at a certain location due to flooding. The individual risk of Zuid Holland varies from 10^{-4} to 10^{-6} persons/year (Vergouwe, 2016). However, the individual risk analysis needs to consider the probability of occurrence of flood scenario i and the mortality at the location given flood scenario i . Since the lack of investigations of these parameters, the individual risk of Shanghai is unclear. To get an insight of the individual risk of Shanghai, a simplified calculation is implemented:

$$IR_{flood} = P_{f-flood} * P_{d/F-flood}$$

In which

$P_{f-flood}$ = actual probability of inundation;

$P_{d/F-flood}$ = conditional probability which means that probability that an individual who lives in the protected coastal region would be killed given occurrence of the sea flood.

As for Shanghai sea dikes, the inundation probability can be taken as the system failure probability calculated in previous ($3.31E-02$ — $3.64E-02$), and the conditional probability is related many factors e.g.: Types of floods: predictable or unpredictable; Evacuation ratio; Warning time, etc. Since there is hardly any information of above factors in Shanghai. Based on historical information, the magnitude of $P_{d/F-flood}$ in Shanghai can be assumed to be $1E-04$. Therefore, the individual risk of Shanghai can be assumed to vary from 10^{-5} to 10^{-6} .

c. Societal risk

The loss-of-life risk considers the number of deaths as a direct result of a flood. Large numbers of fatalities can be expected in areas where lots of people live, or where a very large area may be flooded in a single event. A rare flood with a large number of fatalities has a

greater societal impact than much more frequent, smaller incidents. This is expressed in the form of societal risk, which is illustrated by the probability that 1, 10, 100, 1000 or 10,000 fatalities will occur. Figure 5.9 shows the probability that 1, 10, 100 or 1000 fatalities will occur on Zuid Holland(S. N. Jonkman, Kok, & Vrijling, 2008). An example of the FN curve due to historical floods (1950-2010) in China is shown in Figure 5.10 (Ke, 2014). Since the FN curves for Shanghai are insufficient, so this will need further analysis to get the exact FN curves. In this simple comparison, the China

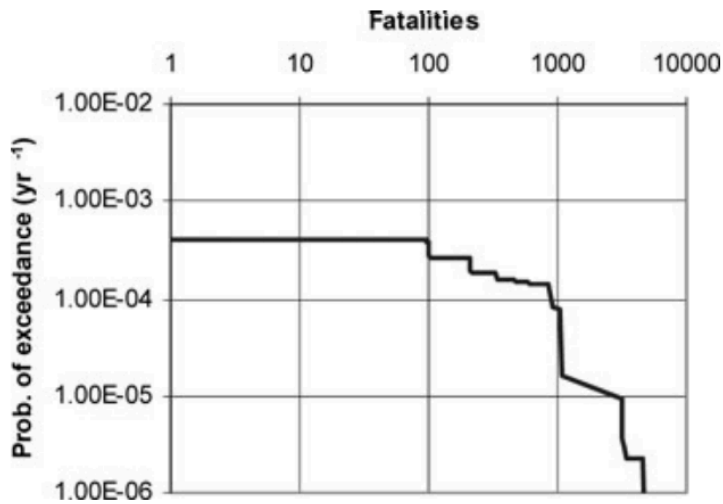


Figure 5.9: FN curve for flooding of Zuid Holland.(S. N. Jonkman et al., 2008)

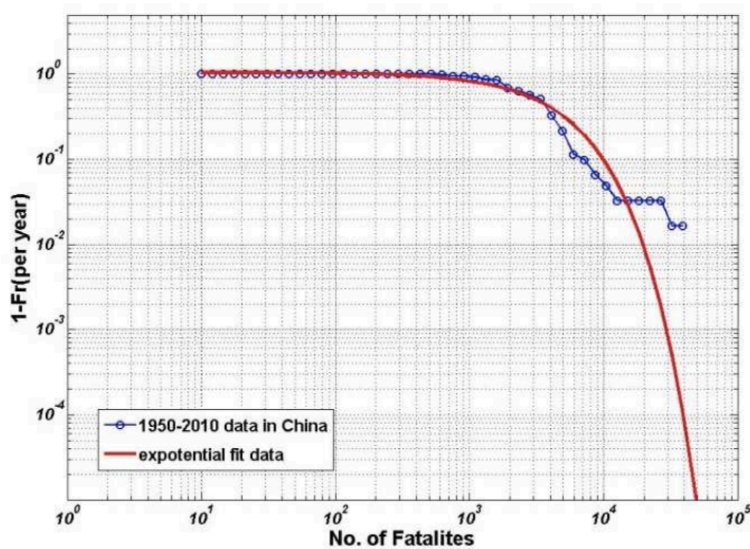


Figure 5.10: Empirical FN curve (1950-2010) due to historical floods in mainland of China(Ke, 2014)

A comparison study between Shanghai and Zuid Holland is conducted in terms of flood risk management in order to give an insight into the safety standard of Shanghai sea dike. The general comparison in terms of geography, individual, societal and economic risk between Shanghai and Zuid Holland is shown in Table 5.8.

Table 5.8: Comparison of Shanghai and Zuid Holland.

	Shanghai	Zuid Holland	Ratio
Area [hectare]	634,000	281,800	2.25
Population [million]	24.3	3.71	6.55
Economic risk [million €/year]	1.7-5.2	2.3	-
Individual risk [persons/year]	10^{-5} - 10^{-6}	10^{-4} - 10^{-6}	-
Societal risk [annual probability of 10,100 and 1000 fatalities]	Figure 5.8	Figure 5.7	around 1000
Safety standard based on cost-benefit analysis	?	1/10,000-1/30,000	-

The comparison between Shanghai and Zuid Holland is not for deriving the safety standard for Shanghai sea dikes, which needs a more complete cost-benefit analysis and economical optimization to find out the optimizing safety standard considering the consequences and the economics. In this study, the comparison is to have a better understanding of safety standard of Shanghai and help compare the dikes in Shanghai to the standards in other place to assess whether the “real” safety level of Shanghai dikes is acceptable or should be increased. Moreover, the comparison of Shanghai and Zuid Holland can also give an insight of the measures for risk reduction.

Since the real safety standard can only be derived by cost-benefit analysis. In this study, three safety standards were chosen to see the differences, 1/10,000 , 1/500, 1/200.

- 1) 1/10,000 is the standard derived from the comparison between Shanghai and Zuid Holland. Since the risks of Shanghai and Zuid Holland do not show significant difference, the safety standard of Zuid Holland can be chosen.
- 2) 1/500 is the highest safety standard in Germany, which is used for special items with extraordinary consequences in the case of flooding(Tourment et al., 2018).
- 3) 1/200 is the design condition of Shanghai sea dikes. Shanghai sea dikes are designed with a 200-year return period water level with 12 level wind speed. In this study, the water level condition and the wave/wind condition are assumed to be 100% dependent, which means that the 200-year return period will occurs together with the 12 level wind speed, so the joint probability of water level and wave/wind of Shanghai sea dikes in design condition can be assumed to be 1/200. Therefore, the 1/200 can be assumed to be one safety standard.

5.4.2 Required level of reliability

After the safety standard deriving, the next step is to assess whether a dike section complies with the standard. Figure 5.11 states the two steps to derive the required failure probability at cross-section level:

1. Determine a required failure probability per failure mechanism
2. Considering the length effect, determine required failure probability per failure mechanism at section level(Kok, Jongejan, Nieuwjaar, & Tanczos, 2017).

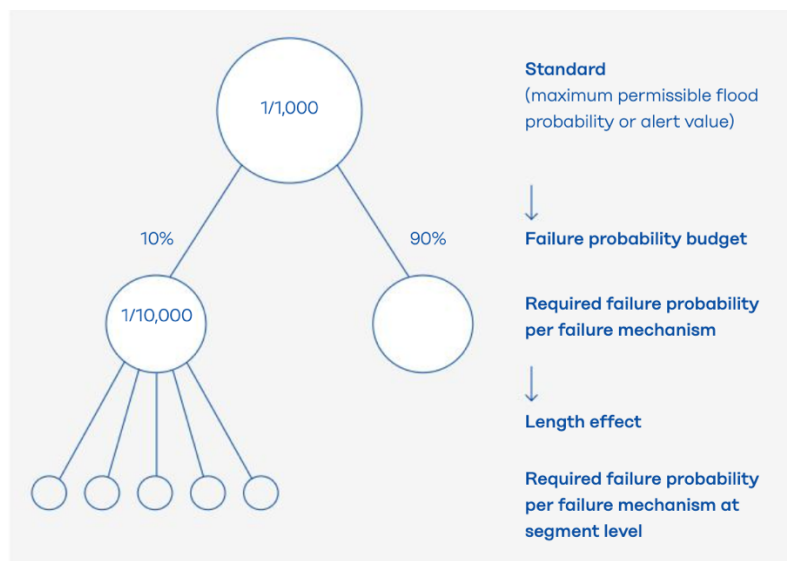


Figure 5.11: From standard to required failure probability per failure mechanism for a representative cross-section(Kok et al., 2017)

The two steps and Figure 5.11 are incorporated in the Formula 5.4, 5.5 which shows how a failure probability for a section i of a flood defence for a specific failure mechanism j can be derived.

$$P_{req,i,j} = \frac{\omega_j}{N_j} \cdot P_{req} \quad (5.4)$$

$$N_j = 1 + \frac{a_j \cdot L}{b_j} \quad (5.5)$$

In which

$P_{req,i,j}$ = required failure probability for section i and failure mechanism j [-]

ω_j = failure probability budget of failure mechanism j [-]

N_j = length effect factor [-]

P_{req} = required failure probability(=safety standard) [-]

a. Failure probability budget

Required failure probability for a failure mechanism at section level is determined by dividing a flood probability standard over different failure mechanisms, which is known as failure probability budget. Figure 5.12 shows the standard failure probability budgets which were drawn up for the Statutory Assessment Instruments 2017.

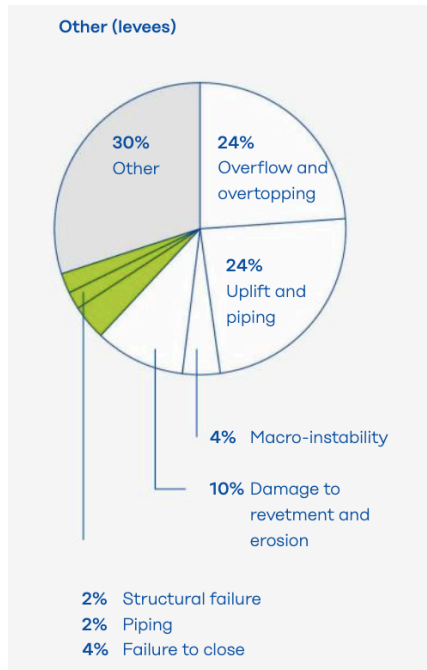


Figure 5.12: The standard failure probability budget(Kok et al., 2017)

Based the standard failure probability budget in the Netherlands and the failure probability result of Shanghai sea dikes, the failure probability budget for Shanghai can be derived shown in Table 5.9. Since the results show that the overtopping is the most dangerous failure mechanism and followed by Macro-instability and revetment failure, the macro-instability budget can be chosen to be 10% and the revetment failure 4%. The budget for other failure mechanism is higher since only three failure mechanism is considered in this study.

Table 5.9: The failure probability budget for Shanghai

Failure mechanism	Failure probability budget
Overtopping/overflow	24%
Macro-instability	10%
Revetment failure	4%
Other	59%

Based on this, the Shanghai sea dike system failure probability that including other failure mechanisms is $8.07E-02$ — $8.88E-02$.

b. Length effect factor

Length effect is defined as the increase of the failure probability when the length of the dike stretch increases (Kanning, 2012). By introducing the length-effect factor N , the target reliability for a specific dike section can be derived.

$$N_j = 1 + \frac{a_j \cdot L}{b_j} \quad (5.5)$$

In which:

N_j = length effect factor [-]

a_j = fraction of the trajectory's length that is sensitive to failure mechanism j [-]

L = length of the trajectory [m]

b_j = length of a typical independent section for failure mechanism j [m]

However, it requires deep investigation which needs extra data and research to deriving the accurate length effect factors.

Based on Kanning's research(Kanning, 2012), the length effect is of minor importance for failure mechanism of overtopping/overflow, so the length factor can take value 1. Same as the overtopping/overflow, the length effect factor can also take as the value 1 for the revetment failure.

On the other hand, resistance will affect macro-instability, which highly depends on the spatial variability of the subsoil, so for macro-instability, the length factor takes a bigger value 10.

Based on these, the required failure probabilities per failure mechanism and the required failure probabilities per failure mechanism at section level can be derived. According to the results calculated before, whether the required failure probabilities per failure mechanism and the required failure probabilities per failure mechanism at section level can be satisfied are shown in Table 5.10 The $P_{required,f}$ means required failure probability per failure mechanism; $P_{required,f,section}$ means required failure probability per failure mechanism at section level

Table 5.10: Required failure probability comparison

Failure mechanism	Overtopping/Overflow		
Safety standard	1/10,000	1/500	1/200
$P_{required,f}$	2.4E-5	4.8E-4	1.2E-3
Whether $P_{required,f}$ can be satisfied	No	No	No
$P_{required,f,section}$	2.4E-5	4.8E-4	1.2E-3
Number of sections satisfy $P_{required,f,section}$	0	1	3
Failure mechanism	Macro-instability		
Safety standard	1/10,000	1/500	1/200
$P_{required,f}$	1E-5	2E-4	5E-4
Whether $P_{required,f}$ can be satisfied	No	No	No
$P_{required,f,section}$	1E-6	2E-5	5E-5
Number of sections satisfy $P_{required,f,section}$	46	79	79
Failure mechanism	Revetment failure		
Safety standard	1/10,000	1/500	1/200
$P_{required,f}$	4E-6	8E-5	2E-4
Whether $P_{required,f}$ can be satisfied	No	No	No
$P_{required,f,section}$	4E-6	8E-5	2E-4
Number of sections satisfy $P_{required,f,section}$	79	79	79

According to the results, the overtopping and macro-instability cannot meet the required failure probability of three safety standards, which means the safety level of Shanghai sea dikes needs to increase.

To see whether the increasing of critical overtopping discharge and crest elevation will influence the safety level of Shanghai sea dikes system, shown in Table 5.11. Based on the results, increasing critical discharge from 1 l/m/s to 5 or 10 l/m/s or increasing the crest elevation of 0.5m or 1m can increase the safety level and 1/200 safety standard can all be satisfied. However, the stricter standards (1/500 and 1/10,000) still cannot be reached.

Table 5.11 The comparison of the safety level results of increasing critical discharge or crest elevation

Safety standard	Whether $P_{required,f}$ can be satisfied		
Safety standard	1/10,000	1/500	1/200
qc=1 l/m/s (Current Situation)	No	No	No
qc=5 l/m/s	No	No	Yes
qc=10 l/m/s	No	No	Yes
Crest elevation+0.5m	No	No	Yes
Crest elevation+1m	No	No	Yes

5.4.3 Risk decrease measures

a. Engineering measures

The crest level of dike is an important variable for failure probability of overtopping, so increase the crest level can be an effective measure to increase the safety level of Shanghai sea dikes. The crest level of most sections of Shanghai sea dikes cannot satisfy the design crest level, and this may be the main reason that failure probability of overtopping is large. The optimizing crest height increase can be derived based on cost-benefit analysis and the economic optimization approach. This engineering measure is widely used in both Shanghai and the Netherlands and it can reduce the risk by reducing the failure probability. Another engineering method that can be used is to strengthen the dike inner slope to increase the critical overtopping discharge, this measure will be a good choice when the cost of heightening is high.

b. Emergency measures

Some temporary measures can be taken to increase the stability of dikes. The failure probability of macro-instability can be reduced by increasing the weight on the resistance side of sliding plane or covering the outer slope to reduce the infiltration of water. These emergency measures are also widely used in both Shanghai and the Netherlands to decrease the failure probability of dike instability.

c. “Soft” measures

Except for engineering measures mentioned above, some “soft” measures can help reduce the flooding consequences to reduce the flood risks. For example, developing an early-warning system can reduce the individual risks and evacuation is also an approach that is used in Shanghai.

Chapter 6 Conclusions and recommendations

6.1 Conclusions

Generally, the objectives of the research have been achieved by the following steps: identifying the most important failure mechanism; analysis of boundary conditions; division of the system into sections; calculation of conditional failure probability and combining into the system failure probability; assessment of safety of Shanghai sea dikes.

6.1.1 Recognitions about the section decomposition

- a. **Overtopping/Overflow, revetment failure, macro-instability are vital failure mechanism.**

Overtopping/overflow, revetment instability and macro-instability are identified as the governing failure mechanisms for Shanghai sea dikes. Overtopping/overflow is the most dangerous failure mechanism, followed by macro-instability.

- b. **Section 35 is the most vulnerable to overtopping/overflow; Section 69-79 are vulnerable to revetment instability.**

Section 35 is the most vulnerable to overtopping/overflow because the crest level of it is lower and the water level is higher than other sections; Section 69-79 are vulnerable to revetment instability because the wave condition is severe.

6.1.2 Combination of failure probability

- a. **The combination of failure probability per failure mechanism**

Combining the failure probability per sections based on the correlations between sections can give the failure probability of the dike system, which can be regarded as a series system. Therefore, the boundaries of the system failure probability can be derived ($3.31E-02$ — $3.64E-02$).

6.1.3 Safety assessment

a. The safety standard analysis

Since there is no clear safety standard for Shanghai sea dike system and only a complete cost-benefit analysis can give the exact safety standard for flood defence system, three different safety standards are used to assess the real safety level of Shanghai sea dikes. Moreover, a comparison between Shanghai and Zuid Holland of the consequences and risks was implemented. They required failure probability at section level of each safety standard can be derived, and the results tell that the safety level of Shanghai sea dikes needs to be increased.

b. Measures of risk reduction

Since the most dangerous failure mechanism is overtopping, reducing the failure probability of overtopping will contribute to the risk reduction of Shanghai sea dikes. Based on sensitivity analysis before, increasing the critical discharge or increasing the crest elevation are two engineering methods that can decrease the overtopping failure probability.

The critical discharge can be increased by strengthening the inner slope. If the critical overtopping discharge increase from 1 l/m/s to 5 l/m/s or 10 l/m/s, the system failure probability(not including the failure probability budget of other failure mechanisms) will increase from $3.31E-2$ — $3.64E-2$ ($q_c=1$ l/m/s) to $5.77E-3$ — $9.18E-3$ ($q_c=5$ l/m/s), $1.68E-3$ — $5.09E-3$ ($q_c=10$ l/m/s). If the crest elevation increase 0.5m or 1m, the system failure probability(not including the failure probability budget of other failure mechanisms) will increase from $3.31E-2$ — $3.64E-2$ (current crest elevation) to $3.05E-3$ — $6.46E-3$ (current crest elevation+0.5m), $1.94E-3$ — $5.35E-3$ (current crest elevation+1m).

6.2 Recommendations

In this study, some assumptions were made due to the insufficient dataset or simplified calculations, which resulted in a conservative failure probability for the Shanghai sea dikes system. In this section, recommendations are given for further research.

- 1) For the reliability analysis of Shanghai flood defence system, the optimizing safety standard based on cost-benefit analysis and economic optimization should be derived first. This will also help the authority to have a better acknowledge of the safety level
- 2) This study gives an estimate of Shanghai sea dikes, which can provide a reference for maintenance and construction work.

- 3) The matlab models used in calculation of failure probability can give an option for failure probability calculation of other regions where the data is not sufficient.
- 4) In this study, due to the limitation of information, several assumptions have been made. To make the results more reliable, additional efforts can be done, like large-scale investigation of the water level and wave conditions, etc.
- 5) In this study, only three main failure mechanisms are included, which may give an underestimated failure probability. Other failure probability can also be analyzed for further work.

Bibliography

- Allsop, W., Kortenhaus, A., Morris, M., Buijs, F., Hassan, R., Young, M., . . . Dyer, M. (2007). Failure mechanisms for flood defence structures. *FLOODsite Report. T04_06_01*.
- Bischiniotis, K. (2013). *Cost optimal river dike design using probabilistic methods*. MSc thesis, Delft University of Technology,
- Bonfantini, F. (2014). *Set-up to design guidance for the Crablock armour unit*. Retrieved from
- Bureau, S. I. o. B. R. (2011). *Planning of Shanghai sea dikes(2011-2020) (in Chinese)*.
- Cai, X. (2017). Safety assessment for macro-stability of Shanghai sea dikes (in Chinese). *Technical Supervision in Water Resources, 25(05)*, 89-92.
- Chen, F., & Qi, D. (2010). Investigation and analysis on the current situation of seawall protection capability in shanghai (in Chinese). *Journal of Marine Sciences, 28(01)*, 72-79.
- Chen, Yong, Shi, Y., Li, B., & Yu, J. (2016). Seawall Subsidence in Shanghai: Characteristics and Driving Mechanisms (in Chinese). *Marine Geology and Quaternary Geology, 36(6)*, 71-78.
- CIRIA. (2013). *The international levee handbook: Ciria*.
- Cui, d., He, Y., & Liu, X. (2018). Discussion on safety appraisal procedure and key technologies for sea dike in Shanghai. *CHINA FLOOD & DROUGHT MANAGEMENT, 28(12)*, 80-85.
- Du, S., Gu, H., Wen, J., Chen, K., & Van Rompaey, A. (2015). Detecting flood variations in Shanghai over 1949–2009 with Mann-Kendall tests and a newspaper-based database. *Water, 7(5)*, 1808-1824.
- Du, X. (2013). Calculation of failure probability of typical seawall in Shanghai Lingang Area. *Shanghai Water, 29*, 48-51.
- en Milieu, M. v. I. (2016a). Regeling veiligheid primaire waterkeringen 2017: Bijlage iii sterkte en veiligheid. In: Den Haag: Ministerie van Infrastructuur en Milieu.
- en Milieu, M. v. I. (2016b). Schematiseringshandleiding grasbekleding. *WBI2017*.
- en Waterstaat, M. v. V., & Waterbouwkunde, D. W.-e. (2005). Veiligheid Nederland in Kaart. *Tussenstand onderzoek overstromingsrisico's. Den Haag*.

- Fan, H. (2006). *Experimental Study on the Overtopping Discharge and Overtopping Flow of the Sloped Seawall*. (Master's thesis). Hohai University,
- Gringorten, I. I. (1963). A plotting rule for extreme probability paper. *Journal of Geophysical Research*, 68(3), 813-814.
- Groot, T. (2015). *Macro-stability safety assessment for flood defenses with buried pipes*. (Master's thesis). University of Twente, Twente.
- Hofland, B., Chen, X., Altomare, C., & Oosterlo, P. (2017). Prediction formula for the spectral wave period $T_{m-1,0}$ on mildly sloping shallow foreshores. *Coastal Engineering*, 123, 21-28.
- Jonkman, S., & Schweckendiek, T. (2015a). *Developments in levee reliability and flood risk analysis in the Netherlands*. Paper presented at the Geotechnical Risk and Safety V; 5th International Symposium on Geotechnical Safety and Risk; Rotterdam (The Netherlands), 13-16 Oct. 2015.
- Jonkman, S., & Schweckendiek, T. (2015b). Flood Defences, Lecture notes CIE5314. *Delft University of Technology*, 105, 106.
- Jonkman, S. N., Kok, M., & Vrijling, J. K. (2008). Flood risk assessment in the Netherlands: A case study for dike ring South Holland. *Risk Analysis: An International Journal*, 28(5), 1357-1374.
- Kanning, W. (2012). *The weakest link: spatial variability in the piping failure mechanism of dikes*.
- Ke, Q. (2014). Flood risk analysis for metropolitan areas—a case study for Shanghai.
- Kok, M., Jongejan, R., Nieuwjaar, M., & Tanczos, I. (2017). Fundamentals of flood protection. *Ministry of Infrastructure and the Environment and the Expertise Network for Flood Protection* https://www.hkv.nl/upload/publication/Fundamentals_of_Flood_Protections_MK_WEBSITE.pdf.
- Li, C. (2015). *The coupling analysis of seawall seepage field-stress field under the influence of tide level*. (Master's thesis). Heifei University of Technology,
- Lin, H., Zhong, W., Xiong, W., & Tang, W. (2014). Slope stability analysis using limit equilibrium method in nonlinear criterion. *The Scientific World Journal*, 2014.
- Manual, R. (2007). The Rock Manual. The use of rock in hydraulic engineering. *CIRIA-CUR, Publication C683*.

- Ministry of Water Resources. (2014). *Code for design of sea dike project*.
- Minoru, M. (1990). *Ground Engineering-Theory of Reliability Design and Its Practice*: China Communications Press.
- Morris, M. (2008). Failure mechanisms for flood defence structures. *Fact sheet T04-08-07, Floodsite*.
- Qiyi, X., & Guangwen, H. (1994). Computation and Verification of Wave Characteristics along the Coastal Water of Yangtze River Estuary and Hangzhou Bay. *Journal of Hohai University*, 000(002), 30-38.
- Shanghai Institute of Building Research Company (2011). *Standard for Meteorological Parameters of Building Wind Environment Design For Shanghai*.
- Shanghai Municipal Bureau of Statistics. (2018). *Shanghai Statistical Yearbook 2018*: China Statistics Press.
- Shanghai Water Engineering design and Research Institute. (2012). *Design code for promoting sedimentation and land reclamation*.
- Slomp, R., Knoeff, H., Bizzarri, A., Bottema, M., & de Vries, W. (2016). *Probabilistic flood defence assessment tools*. Paper presented at the E3S Web of Conferences.
- Song, J., & Der Kiureghian, A. (2003). Bounds on system reliability by linear programming. *Journal of Engineering Mechanics*, 129(6), 627-636.
- Statistics, S. M. B. o. (2018). *Shanghai Statistical Yearbook 2018*: China Statistics Press.
- t Hart, R., De Bruijn, H., & De Vries, G. (2016). *Fenomenologische beschrijving: Faalmechanismen WTI*. Retrieved from
- Tourment, R., Beullac, B., Peeters, P., Pohl, R., Bottema, M., Van, M., & Rushworth, A. (2018). *European and US Levees and Flood Defences Characteristics, Risks and Governance*. irstea,
- Trompille, V., & Eerninck, N. (2011). D-Geo Stability Version 10.1. *Slope stability software for soft soil engineering. Deltares, the Netherlands*.
- Van, C.-M., van Gelder, P., & Vrijling, J. (2007). Probabilistic investigation of failure mechanisms of coastal flood defence structures. *Asian and Pacific Coasts*.
- Van der Meer, J., Allsop, N., Bruce, T., De Rouck, J., Kortenhaus, A., Pullen, T., . . . Zanuttigh, B. (2018). *EurOtop: Manual on wave overtopping of sea defences and*

related structures: an overtopping manual largely based on European research, but for worldwide application (2 ed.).

- van Montfoort, M. (2018). *Safety assessment method for macro-stability of dikes with high foreshores*. (Master's thesis). Delf University of Technology, Delft.
- Van Westen, C., Alkema, D., Damen, M., Kerle, N., & Kingma, N. (2011). Multi-hazard risk assessment. *United Nations University–ITC School on Disaster Geoinformation Management*.
- Vergouwe, R. (2016). *The national flood risk analysis for the Netherlands: Rijkswaterstaat VNK Project Office*.
- Wang, L. (2019). *Simulation of compound coastal flooding in shanghai (in Chinese)*. MSc thesis, Shanghai Normal University,
- Wang, W., Xu, Z., & Li, Q. (2018). Design and construction of deep excavations in Shanghai, China. *Geotechnical Research*, 5(3), 143-161.
- Wang, Z. (2016). *Reliability Analysis for the Flood Defence System along the Huangpu River, Shanghai*. (Master's thesis). Delf University of Technology, Delft.
- Wang, Bo, & Xu, S. (2015). Study on the sea dike layout of Shanghai(in Chinese). *Water Resources Planning and Design*(08), 7-10.
- Yan, K., & Zhang, Q. (2016). Numerical simulation of overtopping on sloping dike with fence panels. *China Harbour Engineering*, v.36;No.216(2), 26-29+47.
- Yin, J. (2020a). *Simulation of flooding due to embankment breaches by Delft3D Flexible Mesh: Case study of coastal area in Shanghai*. (Master's thesis). Delf University of Technology, Delft.
- Yin, J. (2020b). Simulation of flooding due to embankment breaches by Delft3D Flexible Mesh: Case study of coastal area in Shanghai.
- Zhang, J., Chen, L., Wu, H., & Zhao, d. (2015). Study on recent evolution characteristics of the Yangtze River Estuary
. *Journal of Sediment Research*, 2, 74-80.
- Zhang, Z., Wu, W., Wang, B., & Liu, Y. (2012). Numerical Simulation of Overtopping Against Sea Dikes with Fence Panels in Regular Waves. *Chinese Quarterly of Mechanics*, 033(002), 221-230.

AppendixA Deterministic Analysis

To give some support of identifying the governing failure mechanisms, the deterministic analysis can help to have an initial understanding of different failure mechanisms. The Pudong part is chosen as an example, the data that needed are in Chapter 2:

- **Piping**

Piping will occur only if the following two conditions are satisfied: (1) The clay layer under the dike must be ruptured (2) Continuous transport of sand must take place. For case 2, Bligh's method can be used, and limit state function can be written as:

$$FoS = L/cH$$

In Which

L = seepage length (m). Here, it is chosen as length of dike base;

c = coefficient for safety design, which can be seen in the figure below

H = difference in water levels between seaside and inland (m).

In this section, L = 85.9 m, c=3 for clay, H = 6.27 m, so

$$FoS = 4.57 > 1$$

- **Shearing**

Simplifying the cross-section and calculate the water pressure and shear capacity

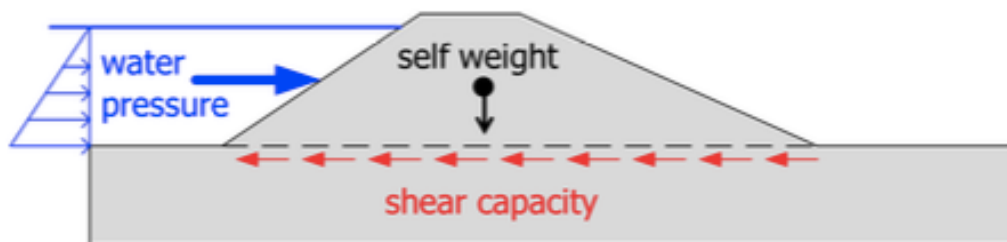


Figure A.1: Schematic illustration of horizontal sliding of the dike body (shearing of the base). The driving force is the horizontal water pressure exerted by the outside water (i.e. river, canal or lake), which may overcome the shear capacity of the dike base (S. Jonkman & Schweckendiek, 2015b).

$$Z = fW/P$$

In which

W = self-weight of dike body(kN);

P = water pressure(kN);

f = friction coefficient.

In this section, $W=5967.27\text{kN}$, $P=192.8\text{kN}$, $f=\tan\Phi=0.56$, so

$$FoS = 17.33 > 1$$

Appendix B Roughness factor

The typical outer slope revetment material in Shanghai is fence board(concrete) shown in the figure below. There are no data for the roughness factor of the fence board, but several researchers do some studies on it.

Fan Hongxia(2006) carried out a series of physical experimentations to study diversified parameters affecting the overtopping discharge, and the effect of fence board is shown in the figure: (Fan, 2006)

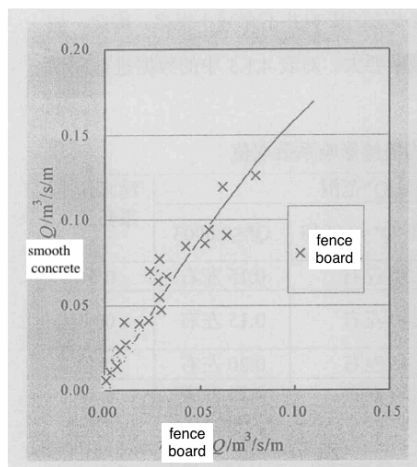


Figure B.1: The overtopping rate of different revetment materials(Fan, 2006)

Yan Kedi, Zhang Qinghe(2016) established a numerical model of overtopping using the numerical wave tank, simulated the overtopping on a smooth slope dike under regular waves based on the open source software OpenFOAM. The results are compared with physical model experiment data, which proved that the results are in good agreement with the experimental data, which verifies the reasonably of the numerical model. By comparing the overtopping discharges on slopes with and without fence panels, they obtained that the overtopping discharge friction(compared with the concrete revetment) of fence panels is 0.81(Yan & Zhang, 2016) the result is similar to the previous one from FAN Hong xia (2006)

	T /s	revetment	overtopping discharge $Q/10^{-2}$	ratio
physical experiment data	1.2	concrete	3.78	0.78
		fence board	2.96	
	1.8	concrete	6.51	0.85
		fence board	5.50	
numerical simulation	1.2	concrete	3.60	0.81
		fence board	2.91	
	1.8	concrete	6.40	0.82
		fence board	5.23	

Figure B.2: Comparison of overtopping numerical results and experiment results.(Yan & Zhang, 2016)

Zhang Zhijie, WU Wei, Wang Benlong, Liu Hua(2012), established a numerical wave tank based on the Reynolds-averaged Navier-Stokes equation, the Volume of Fluid method and the RNG k- ϵ turbulence model, for the case of a sea dike with fence panels, the computed overtopping discharge and the depth averaged velocity of overtopping flows on the dike crest were obtained and compared with the physical model result. The results implied that the fence board contributes to the dissipation of overtopping velocity and overtopping discharge, and the reduction factor is 0.8 compared to the concrete revetment. (Z. Zhang, Wu, Wang, & Liu, 2012)

In the conclusion of these studies, the roughness influence of fence board can be calculated by:

$$q_{fence\ board} = 0.8 \times q_{concrete}$$

AppendixC Seepage analysis based on SEEP/W

- Parameters of dike material

Although the cross-sections of five sub-division are different, the materials of dike body are similar. According to the existing surveys and related literatures, the mechanical parameters of the dike body material are similar to Shanghai gray sandy clay, so the horizontal coefficient of permeability $k_x = 2.5 \times 10^{-6} \text{ m/s}$, vertical coefficient of permeability $k_z = 1.2 \times 10^{-6} \text{ m/s}$, unit weight $\gamma=1.92 \text{ kN/m}^3$ and coefficient of compressibility=0.18/MPa(Li, 2015). The permeability parameters used in the Seep/w are assumed to be deterministic value since the Seep/w model can only set up of deterministic initial input data.

- Boundary condition

The boundary conditions of sea dikes are complicated due to the tide effect, it will change with time. Tide level will change a lot in a short time, so a large amount of tide data is required in order to model accurate seepage. However, the tide data for Shanghai are insufficient. Conglei Li did some studies about the influence of rapid change of tidal level on the phreatic lines in Shanghai sea dikes. He chose one tide level change process on 12th October,2004 and modelled the effect of rapid tide level rise and drop on the phreatic line. The results shows that the phreatic line only follows the change of tide level on a small part on the water side, which are in Figure 6.6.(Li, 2015)

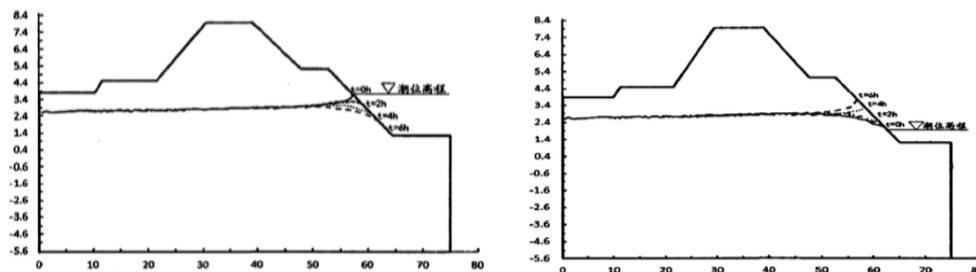


Figure C.1: The effect of tidal level change on phreatic line (Left: changing curves of free surface when tide level rises; Right: The changing curves of free surface when tide level drops) (Li, 2015)

The phreatic line not varies a lot with the change of tide level on the land side, so the effect on the inner slope stability may not be affected a lot due to the change of phreatic line.

For the seepage in this study, the boundary condition can be assumed to be constant water level in Chapter 2.